Probabilistic Engineering Mechanics 69 (2022) 103319

Contents lists available at ScienceDirect

Probabilistic Engineering Mechanics

journal homepage: www.elsevier.com/locate/probengmech

# A quadratic Wiener path integral approximation for stochastic response determination of multi-degree-of-freedom nonlinear systems

Ying Zhao [a], Apostolos F. Psaros [b], Ioannis Petromichelakis [c], Ioannis A. Kougioumtzoglou [c,*]

[a] Key Laboratory of Air-driven Equipment of Zhejiang Province & College of Mechanical Engineering, Quzhou University, Quzhou, 324000, China
[b] Division of Applied Mathematics, Brown University, Providence, RI 02906, United States
[c] Department of Civil Engineering and Engineering Mechanics, Columbia University, 500 W 120th St, New York, NY 10027, United States

ARTICLE INFO

*Keywords:*
Wiener path integral
Quadratic approximation
Functional series expansions
Most probable path
Nonlinear systems
Stochastic dynamics

ABSTRACT

A Wiener path integral (WPI) technique is developed for determining the stochastic response of multi-degree-of-freedom (MDOF) nonlinear systems. Specifically, the nonlinear system response joint transition probability density function (PDF) is expressed as a WPI over the space of paths satisfying the initial and final conditions in time. Next, a functional series expansion is considered for the WPI and a quadratic approximation is employed. Further, relying on a variational principle yields a functional optimization problem to be solved for the most probable path, which is used for determining approximately the joint response transition PDF. It is shown that compared to the standard (semiclassical) WPI solution approach, which accounts only for the most probable path, the quadratic approximation developed herein exhibits enhanced accuracy. This is due to the fact that fluctuations around the most probable path are also accounted for by considering a localized state-dependent factor in the calculation of the WPI. Furthermore, the PDF normalization step of the most probable path approach is bypassed, and thus, probabilities of rare events (e.g., failures) can be determined in a direct manner without the need for obtaining the complete joint response PDF first. The herein developed technique can be construed as an extension of earlier efforts in the literature to account for MDOF systems. Several numerical examples are considered for demonstrating the accuracy of the technique. These pertain to various dynamical systems exhibiting diverse nonlinear behaviors. Comparisons with pertinent Monte Carlo simulation data are included as well.

## 1. Introduction

Irrespective of the scale of the problem, persistent challenges in the field of stochastic engineering dynamics exist. Indicatively, these pertain to high dimensionality, complex nonlinear/hysteretic behaviors, as well as to non-white and non-Gaussian stochastic excitation modeling. In this regard, the state-of-the-art solution techniques for determining system response and reliability statistics can be broadly divided into two categories; see also [1–3] for a broad perspective.

First, there are techniques that exhibit a high degree of accuracy, but the associated computational cost becomes prohibitive with increasing number of stochastic dimensions. For example, numerical schemes have been developed over the past three decades that rely on a discrete form of the Chapman–Kolmogorov equation for propagating the system response probability density function (PDF) in short time steps (e.g., [4–7]). However, although they exhibit excellent accuracy in predicting even the tails of the system response PDF, their performance is hindered eventually by excessive computational cost with increasing dimensionality (e.g., [8]). This is due to the fact that a multi-convolution integral needs to be computed for each and every time step, while the requisite time increment must remain short; see also [9] for a recent review paper.

Second, there are techniques that can readily treat high-dimensional systems, but provide reliable estimates for low-order response statistics only. Indicatively, statistical linearization has been one of the most versatile and popular approximate approaches for determining the stochastic response of nonlinear systems in a computationally efficient manner (e.g., [1,10]). Nevertheless, primarily due to the Gaussian response assumption, the standard approach is generally restricted to the determination of first- and second-order response statistics only; see also [11,12] for some recent extensions referring to joint time–frequency analysis and to systems with singular parameter matrices, respectively.

Clearly, the development of versatile solution techniques that exhibit both high accuracy and low computational cost is critical for addressing the aforementioned challenges, and for advancing the field of stochastic engineering dynamics further. One of the promising solution techniques, recently pioneered in the field of engineering mechanics by Kougioumtzoglou and co-workers (e.g., [13–15]), relates to the

* Corresponding author.
*E-mail address:* ikougioum@columbia.edu (I.A. Kougioumtzoglou).

https://doi.org/10.1016/j.probengmech.2022.103319
Received 25 April 2022; Accepted 14 June 2022
Available online 20 June 2022

concept of a path integral that was originally developed by Norbert Wiener [16]; see also [17] for an indicative standard book referring to theoretical physics applications.

According to the Wiener path integral (WPI) technique (e.g., [18]), the system response joint transition PDF is expressed as a functional integral over the space of all possible paths satisfying the initial and final conditions in time. Next, since this functional integral is rarely amenable to analytical evaluation, an approximate calculation is required. This has been pursued by employing a functional integral series expansion and by considering the contribution only of the first term pertaining to the path with the maximum probability of occurrence. This is referred to in the literature as the most probable path and corresponds to an extremum of the functional integrand. In this regard, the most probable path is determined by solving a functional minimization problem that takes the form of a deterministic boundary value problem (BVP) [19], and is used for determining approximately the system response joint transition PDF. Note that the WPI technique is capable of handling complex stochastic excitation modeling and systems with diverse nonlinear/hysteretic behaviors [18,20–22]. Further, high-dimensional systems can be readily treated by relying on a variational formulation with mixed fixed/free boundary conditions, which renders the computational cost independent of the total number of stochastic dimensions [23]. Furthermore, it was shown in [24] that the associated computational cost can be reduced drastically by employing sparse representations for the system response PDF in conjunction with compressive sampling schemes and group sparsity concepts [25].

In this paper, the accuracy degree exhibited by the WPI technique is enhanced by considering higher order terms in the functional series expansion. Specifically, fluctuations around the most probable path are also accounted for by employing a quadratic WPI approximation. Compared to the standard most probable path approach, this novel solution treatment introduces a localized state-dependent factor in the approximate evaluation of the system response joint transition PDF. Thus, the nonlinear system stochastic response is determined more accurately. Further, the aforementioned localization capability renders the technique particularly suitable for structural reliability assessment applications, where estimating probabilities of failure events is associated with determining only specific portions of the response PDF, such as the tails. The herein developed technique can be construed as an extension of the results in [26] to account for multi-degree-of-freedom (MDOF) systems. Several numerical examples are considered for demonstrating the accuracy of the technique. These pertain to various dynamical systems exhibiting diverse nonlinear behaviors. Comparisons with pertinent Monte Carlo simulation data are included as well.

## 2. Preliminaries

### 2.1. Wiener path integral formulation

In this section, the main aspects of the WPI formalism in conjunction with a stochastically excited MDOF nonlinear system are presented for completeness. The interested reader is also directed to [23,27] for more details. Next, consider an $m$-DOF nonlinear oscillator whose dynamics is governed by

$$\boldsymbol{M}\ddot{\boldsymbol{x}} + \boldsymbol{C}\dot{\boldsymbol{x}} + \boldsymbol{K}\boldsymbol{x} + \boldsymbol{g}(\boldsymbol{x}, \dot{\boldsymbol{x}}) = \boldsymbol{w}(t) \tag{1}$$

where $\boldsymbol{x}$ is the displacement vector process ($\boldsymbol{x} = [x_1, \dots, x_m]^T$); $\boldsymbol{M}$, $\boldsymbol{C}$, $\boldsymbol{K}$ correspond to the $m \times m$ mass, damping and stiffness matrices, respectively; $\boldsymbol{g}(\boldsymbol{x}, \dot{\boldsymbol{x}})$ denotes an arbitrary nonlinear vector function; and $\boldsymbol{w}(t)$ is a white noise stochastic vector process with $\mathbb{E}[\boldsymbol{w}(t_l)] = \boldsymbol{0}$ and $\mathbb{E}[\boldsymbol{w}(t_l)\boldsymbol{w}^T(t_l - t_{l+1})] = \boldsymbol{S_w}\delta(t_l - t_{l+1})$, where $\boldsymbol{S_w} \in \mathbb{R}^{m\times m}$ is an arbitrary, non-singular, symmetric coefficient matrix, and $t_l$, $t_{l+1}$ are two arbitrary time instants.

Further, Eq. (1) can be expressed in the state-variable form

$$\dot{\boldsymbol{\alpha}} = \boldsymbol{A}(\boldsymbol{\alpha}, t) + \boldsymbol{B}(\boldsymbol{\alpha}, t)\boldsymbol{\eta}(t) \tag{2}$$

by setting

$$\boldsymbol{\alpha} = \begin{bmatrix} \boldsymbol{x} \\ \dot{\boldsymbol{x}} \end{bmatrix} = \begin{bmatrix} \boldsymbol{x} \\ \boldsymbol{v} \end{bmatrix} = \begin{bmatrix} \boldsymbol{\alpha}_1 \\ \boldsymbol{\alpha}_2 \end{bmatrix} \tag{3}$$

$$\boldsymbol{A}(\boldsymbol{\alpha}, t) = \begin{bmatrix} \boldsymbol{v} \\ \boldsymbol{M}^{-1}\left(-\boldsymbol{C}\boldsymbol{v} - \boldsymbol{K}\boldsymbol{x} - \boldsymbol{g}(\boldsymbol{x}, \boldsymbol{v})\right) \end{bmatrix} = \begin{bmatrix} \boldsymbol{A}_1 \\ \boldsymbol{A}_2 \end{bmatrix} \tag{4}$$

and

$$\boldsymbol{B}(\boldsymbol{\alpha}, t) = \begin{bmatrix} \boldsymbol{0}_{m\times m} & \boldsymbol{0}_{m\times m} \\ \boldsymbol{0}_{m\times m} & \boldsymbol{M}^{-1}\sqrt{\boldsymbol{S_w}} \end{bmatrix} \tag{5}$$

In Eq. (2), $\boldsymbol{\eta}$ denotes a zero-mean and delta-correlated process of intensity one (e.g., [28]), and in Eq. (5) the square root of matrix $\boldsymbol{S_w}$ is given by $\sqrt{\boldsymbol{S_w}}\sqrt{\boldsymbol{S_w}}^T = \boldsymbol{S_w}$. Clearly, the $m$-dimensional second-order stochastic differential equation (SDE) of Eq. (1) becomes a $2m$-dimensional first-order SDE in Eq. (2) for the process $\boldsymbol{\alpha} = [\boldsymbol{x}, \dot{\boldsymbol{x}}]^T = [\boldsymbol{\alpha}_1, \boldsymbol{\alpha}_2]^T$. Furthermore, the singularity of matrices $\boldsymbol{B}$ and $\widetilde{\boldsymbol{B}} = \boldsymbol{B}\boldsymbol{B}^T$ can be bypassed by introducing an auxiliary variable $\beta \to 0$, and expressing $\boldsymbol{B}$ as

$$\boldsymbol{B} = \begin{bmatrix} \sqrt{\beta}\boldsymbol{I}_{m\times m} & \boldsymbol{0}_{m\times m} \\ \boldsymbol{0}_{m\times m} & \boldsymbol{M}^{-1}\sqrt{\boldsymbol{S_w}} \end{bmatrix} \tag{6}$$

This yields

$$\widetilde{\boldsymbol{B}} = \begin{bmatrix} \beta\boldsymbol{I}_{m\times m} & \boldsymbol{0}_{m\times m} \\ \boldsymbol{0}_{m\times m} & \hat{\boldsymbol{B}} \end{bmatrix} \tag{7}$$

where $\boldsymbol{I}_{m\times m}$ denotes the $m \times m$ identity matrix and the sub-matrix $\hat{\boldsymbol{B}}$ is equal to

$$\hat{\boldsymbol{B}} = \boldsymbol{M}^{-1}\boldsymbol{S_w}\left[\boldsymbol{M}^T\right]^{-1} \tag{8}$$

Note that the determinant and inverse of $\widetilde{\boldsymbol{B}}$ are given, respectively, by

$$\det\widetilde{\boldsymbol{B}} = \beta^m \det\hat{\boldsymbol{B}}, \qquad \widetilde{\boldsymbol{B}}^{-1} = \begin{bmatrix} \frac{1}{\beta}\boldsymbol{I}_{m\times m} & \boldsymbol{0}_{m\times m} \\ \boldsymbol{0}_{m\times m} & \hat{\boldsymbol{B}}^{-1} \end{bmatrix} \tag{9}$$

Next, as $\epsilon = t_{l+1} - t_l \to 0$, the transition PDF related to the SDE of Eq. (2) has been shown to admit a Gaussian distribution of the form

$$p(\boldsymbol{\alpha}_{l+1}, t_{l+1}|\boldsymbol{\alpha}_l, t_l) = \left[\sqrt{(2\pi\epsilon)^{2m}\det\left[\widetilde{\boldsymbol{B}}(\boldsymbol{\alpha}_l, t_l)\right]}\right]^{-1} \times \exp\left(-\frac{1}{2}\frac{[\boldsymbol{\alpha}_{l+1} - \boldsymbol{\alpha}_l - \epsilon\boldsymbol{A}(\boldsymbol{\alpha}_l, t_l)]^T\left[\widetilde{\boldsymbol{B}}(\boldsymbol{\alpha}_l, t_l)\right]^{-1}[\boldsymbol{\alpha}_{l+1} - \boldsymbol{\alpha}_l - \epsilon\boldsymbol{A}(\boldsymbol{\alpha}_l, t_l)]}{\epsilon}\right) \tag{10}$$

In passing, it is remarked that the choice of Eq. (10) as a candidate for the short-time transition PDF is not restrictive, and other alternative non-Gaussian forms can be used (e.g., [29,30]). Substituting Eq. (9) into Eq. (10), and denoting $\boldsymbol{A}_2(\boldsymbol{\alpha}_l, t_l)$ as $\boldsymbol{A}_{2l}$ for simplicity, the short-time transition PDF becomes

$$p\left(\boldsymbol{\alpha}_{l+1}, t_{l+1}|\boldsymbol{\alpha}_l, t_l\right) = \lim_{\substack{\epsilon\to 0\\ \beta\to 0}}\left\{\frac{1}{\sqrt{(2\pi\epsilon\beta)^m}}\exp\left(-\frac{1}{2\beta}\left[\boldsymbol{v}_l - \dot{\boldsymbol{x}}_l\right]^T\left[\boldsymbol{v}_l - \dot{\boldsymbol{x}}_l\right]\epsilon\right) \times\frac{1}{\sqrt{(2\pi\epsilon)^m\det\hat{\boldsymbol{B}}}}\exp\left(-\frac{1}{2}\left[\dot{\boldsymbol{v}}_l - \boldsymbol{A}_{2l}\right]^T\hat{\boldsymbol{B}}^{-1}\left[\dot{\boldsymbol{v}}_l - \boldsymbol{A}_{2l}\right]\epsilon\right)\right\} \tag{11}$$

where $\boldsymbol{v}_l = (\boldsymbol{x}_{l+1} - \boldsymbol{x}_l)/\epsilon$, $\dot{\boldsymbol{v}}_l = (\dot{\boldsymbol{x}}_{l+1} - \dot{\boldsymbol{x}}_l)/\epsilon$, and $\left[\boldsymbol{v}_l - \dot{\boldsymbol{x}}_l\right]^T\left[\boldsymbol{v}_l - \dot{\boldsymbol{x}}_l\right] = \sum_{j=1}^m (v_{jl} - \dot{x}_{jl})^2$.

Further, consider the probability of the process $\boldsymbol{\alpha}$ propagating through some infinitesimally thin tube surrounding a path $\boldsymbol{\alpha}(t)$, $\forall\ t \in [t_i, t_f]$, with fixed initial and final states $\{t_i, \boldsymbol{\alpha}_i\}$ and $\{t_f, \boldsymbol{\alpha}_f\}$, respectively. This can be construed as the probability of the compound event that the path $\boldsymbol{\alpha}(t)$ successively passes through "gates" corresponding to specific time instants; see also [17]. Next, relying on the Markov properties of $\boldsymbol{\alpha}(t)$, the probability of the compound event is expressed, equivalently, as the product of the probabilities corresponding to the independent events. Note that the independent events are described by Eq. (11), and thus, the product of the probabilities takes the form

$$\mathcal{P}[\boldsymbol{\alpha}(t)] = \lim_{\substack{\epsilon\to 0\\ \beta\to 0}} \left\{ \left[ \prod_{l=0}^{L}\prod_{j=1}^{m} \frac{1}{\sqrt{2\pi\beta\epsilon}} \exp\left( \frac{1}{2\beta}(v_{jl} - \dot{x}_{jl})^2 \epsilon \right) \right] \right. \times \left[ \prod_{l=1}^{L}\prod_{j=1}^{2m} \mathrm{d}\alpha_{jl} \right] \left. \times \left[ \prod_{l=0}^{L} \frac{1}{\sqrt{(2\pi\epsilon)^m \det \hat{\boldsymbol{B}}}} \exp\left( -\frac{1}{2} \left[ \dot{\boldsymbol{v}}_l - \boldsymbol{A}_{2l} \right]^T \hat{\boldsymbol{B}}^{-1} \left[ \dot{\boldsymbol{v}}_l - \boldsymbol{A}_{2l} \right] \epsilon \right) \right] \right\} \tag{12}$$

In Eq. (12), the time domain is discretized into $L+2$ points, $\epsilon$ apart (with $L \to \infty$ as $\epsilon \to 0$), i.e.,

$$t_i = t_0 < t_1 < \cdots < t_{L+1} = t_f \tag{13}$$

and the path $\boldsymbol{\alpha}(t)$ is represented by its values $\boldsymbol{\alpha}_l$ at the discrete time points $t_l$, for $l \in \{0,\dots,L+1\}$. Also, $\mathrm{d}\alpha_{jl}$ denote the (infinite in number) infinitesimal gates through which the path propagates. Note that the number of probabilities multiplied in Eq. (12) is equal to $L+1$, whereas the number of gates is $L$, since the final point $\boldsymbol{\alpha}_f$ is fixed.

Next, it is rather intuitive to argue that the respective probabilities of each and every path need to be accounted for, and loosely speaking, "summed up" to evaluate the total probability of the process $\boldsymbol{\alpha}$ starting from $\boldsymbol{\alpha}_i$ at time $t_i$ and ending up at $\boldsymbol{\alpha}_f$ at time $t_f$ (e.g., [17]). In this regard, by utilizing Eq. (12), the joint transition PDF is expressed in the form

$$p\left(\boldsymbol{\alpha}_f, t_f | \boldsymbol{\alpha}_i, t_i\right) = \lim_{\substack{\epsilon\to 0\\ \beta\to 0}} \int_{-\infty}^{\infty} \cdots \int_{-\infty}^{\infty} \left\{ \left[ \prod_{l=0}^{L}\prod_{j=1}^{m} \frac{1}{\sqrt{2\pi\beta\epsilon}} \exp\left( \frac{1}{2\beta}(v_{jl} - \dot{x}_{jl})^2 \epsilon \right) \right] \times \left[ \prod_{l=1}^{L}\prod_{j=1}^{m} \mathrm{d}x_{jl}\mathrm{d}\dot{x}_{jl} \right] \right. \left. \times \left[ \prod_{l=0}^{L} \frac{1}{\sqrt{(2\pi\epsilon)^m \det \hat{\boldsymbol{B}}}} \right] \exp\left( -\sum_{l=0}^{L} \frac{1}{2} \left[ \dot{\boldsymbol{v}}_l - \boldsymbol{A}_{2l} \right]^T \hat{\boldsymbol{B}}^{-1} \left[ \dot{\boldsymbol{v}}_l - \boldsymbol{A}_{2l} \right] \epsilon \right) \right\} \tag{14}$$

Further, defining $\tilde{x}_{j1} = x_{j0} + \dot{x}_{j0}\epsilon$ and $(x_{j1} - \tilde{x}_{j1})/\epsilon = v_{j0} - \dot{x}_{j0}$, and employing the Dirac delta function relationships

$$\lim_{\beta\epsilon\to 0} \frac{1}{\sqrt{2\pi\beta\epsilon}} \exp\left( -\frac{1}{2\beta\epsilon}(x_{j1} - \tilde{x}_{j1})^2 \right) = \delta(x_{j1} - \tilde{x}_{j1}) \tag{15}$$

and

$$\lim_{\beta/\epsilon\to 0} \frac{1}{\sqrt{2\pi(\beta/\epsilon)}} \exp\left( -\frac{1}{2(\beta/\epsilon)}(v_{jl} - \dot{x}_{jl})^2 \right) = \delta(v_{jl} - \dot{x}_{jl}) \tag{16}$$

for every $j \in \{1,\dots,m\}$ and for every $l \in \{0,\dots,L\}$, Eq. (14) becomes

$$p\left(\boldsymbol{\alpha}_f, t_f | \boldsymbol{\alpha}_i, t_i\right) = \lim_{\substack{\epsilon\to 0\\ \beta\to 0}} \int_{-\infty}^{\infty} \cdots \int_{-\infty}^{\infty} \left\{ \left[ \prod_{l=0}^{L} \frac{1}{\sqrt{(2\pi\epsilon)^m \det \hat{\boldsymbol{B}}}} \right] \times \left[ \prod_{l=2}^{L}\prod_{j=1}^{m} \mathrm{d}x_{jl} \right] \times \left[ \prod_{j=1}^{m} \delta(x_{j1} - \tilde{x}_{j1})\mathrm{d}x_{j1} \right] \times \left[ \prod_{l=1}^{L}\prod_{j=1}^{m} \frac{1}{\epsilon}\delta(v_{jl} - \dot{x}_{jl})\mathrm{d}\dot{x}_{jl} \right] \right. \left. \times \exp\left( -\sum_{l=0}^{L} \frac{1}{2} \left[ \dot{\boldsymbol{v}}_l - \boldsymbol{A}_{2l} \right]^T \hat{\boldsymbol{B}}^{-1} \left[ \dot{\boldsymbol{v}}_l - \boldsymbol{A}_{2l} \right] \epsilon \right) \right\} \tag{17}$$

Furthermore, performing $m$ integrations over the variables $x_{11},\dots,x_{m1}$ and $mL$ integrations over the variables $\dot{x}_{11},\dots,\dot{x}_{m1},\dot{x}_{12},\dots,\dot{x}_{m2},\dots,\dot{x}_{1L},\dots,\dot{x}_{mL}$ yields

$$p\left(\boldsymbol{\alpha}_f, t_f | \boldsymbol{\alpha}_i, t_i\right) = \lim_{\substack{\epsilon\to 0\\ \beta\to 0}} \int_{-\infty}^{\infty} \cdots \int_{-\infty}^{\infty} \left\{ \left[ \prod_{l=0}^{L} \frac{1}{\sqrt{(2\pi\epsilon)^m \det \hat{\boldsymbol{B}}}} \right] \times \left[ \prod_{l=2}^{L}\prod_{j=1}^{m} \mathrm{d}x_{jl} \right] \times \frac{1}{\epsilon^{mL}} \exp\left( -\sum_{l=0}^{L} \frac{1}{2} \left[ \dot{\boldsymbol{v}}_l - \boldsymbol{A}_{2l} \right]^T \hat{\boldsymbol{B}}^{-1} \left[ \dot{\boldsymbol{v}}_l - \boldsymbol{A}_{2l} \right] \epsilon \right) \right\} \tag{18}$$

with the constraint $x_{j1} = x_{j0} + v_{j0}\epsilon$ for every $j \in \{1,\dots,m\}$. Next, Eq. (18) converges in the continuous limit to a functional integral (e.g., [17]) over the space of paths $\mathcal{C}\{\boldsymbol{\alpha}_i, t_i; \boldsymbol{\alpha}_f, t_f\}$ with initial state $\boldsymbol{\alpha}_i$ at time $t_i$ and final state $\boldsymbol{\alpha}_f$ at time $t_f$. This takes the form

$$p(\boldsymbol{\alpha}_f, t_f | \boldsymbol{\alpha}_i, t_i) = \int_{\mathcal{C}\{\boldsymbol{\alpha}_i, t_i; \boldsymbol{\alpha}_f, t_f\}} \exp\left( -\int_{t_i}^{t_f} \mathcal{L}[\boldsymbol{\alpha}, \dot{\boldsymbol{\alpha}}]\,\mathrm{d}t \right) \mathcal{D}[\boldsymbol{\alpha}(t)] \tag{19}$$

or, alternatively,

$$p(\boldsymbol{\alpha}_f, t_f | \boldsymbol{\alpha}_i, t_i) = \int_{\mathcal{C}\{\boldsymbol{\alpha}_i, t_i; \boldsymbol{\alpha}_f, t_f\}} \exp\left(-\mathcal{S}[\boldsymbol{\alpha}, \dot{\boldsymbol{\alpha}}]\right) \mathcal{D}[\boldsymbol{\alpha}(t)] \tag{20}$$

where $\mathcal{L}(\boldsymbol{\alpha}, \dot{\boldsymbol{\alpha}})$ denotes the Lagrangian functional of the system expressed as

$$\mathcal{L}(\boldsymbol{\alpha}, \dot{\boldsymbol{\alpha}}) = \frac{1}{2} \left[ \ddot{\boldsymbol{x}} - \boldsymbol{A}_2(\boldsymbol{\alpha}, t) \right]^T \hat{\boldsymbol{B}}^{-1} \left[ \ddot{\boldsymbol{x}} - \boldsymbol{A}_2(\boldsymbol{\alpha}, t) \right] \tag{21}$$

and $\mathcal{D}[\boldsymbol{\alpha}(t)]$ is a functional measure given by

$$\mathcal{D}[\boldsymbol{\alpha}(t)] = \lim_{\epsilon\to 0} \frac{1}{\epsilon^{mL}} \prod_{l=0}^{L} \frac{1}{\sqrt{(2\pi\epsilon)^m \det \hat{\boldsymbol{B}}}} \prod_{l=2}^{L}\prod_{j=1}^{m} \mathrm{d}x_{jl} \tag{22}$$

Comparing Eqs. (19) and (20), the stochastic action $\mathcal{S}[\boldsymbol{\alpha}, \dot{\boldsymbol{\alpha}}]$ is given by

$$\mathcal{S}[\boldsymbol{\alpha}, \dot{\boldsymbol{\alpha}}] = \int_{t_i}^{t_f} \mathcal{L}[\boldsymbol{\alpha}, \dot{\boldsymbol{\alpha}}]\,\mathrm{d}t \tag{23}$$

Further, the joint transition PDF in Eq. (20) can be equivalently written as

$$p\left(\boldsymbol{x}_f, \dot{\boldsymbol{x}}_f, t_f | \boldsymbol{x}_i, \dot{\boldsymbol{x}}_i, t_i\right) = \int_{\mathcal{C}\{\boldsymbol{x}_i, \dot{\boldsymbol{x}}_i, t_i; \boldsymbol{x}_f, \dot{\boldsymbol{x}}_f, t_f\}} \exp\left(-\mathcal{S}[\boldsymbol{x}, \dot{\boldsymbol{x}}, \ddot{\boldsymbol{x}}]\right) \mathcal{D}[\boldsymbol{x}(t)] \tag{24}$$

where

$$\mathcal{S}[\boldsymbol{x}, \dot{\boldsymbol{x}}, \ddot{\boldsymbol{x}}] = \int_{t_i}^{t_f} \mathcal{L}[\boldsymbol{x}, \dot{\boldsymbol{x}}, \ddot{\boldsymbol{x}}]\,\mathrm{d}t \tag{25}$$

The Lagrangian in Eq. (22) is expressed with respect to the process $\boldsymbol{x}$ as

$$\mathcal{L}[\boldsymbol{x}, \dot{\boldsymbol{x}}, \ddot{\boldsymbol{x}}] = \frac{1}{2} \left[ \boldsymbol{M}\ddot{\boldsymbol{x}} + \boldsymbol{C}\dot{\boldsymbol{x}} + \boldsymbol{K}\boldsymbol{x} + \boldsymbol{g}(\boldsymbol{x}, \dot{\boldsymbol{x}}) \right]^T \boldsymbol{S}_{\boldsymbol{w}}^{-1} \times \left[ \boldsymbol{M}\ddot{\boldsymbol{x}} + \boldsymbol{C}\dot{\boldsymbol{x}} + \boldsymbol{K}\boldsymbol{x} + \boldsymbol{g}(\boldsymbol{x}, \dot{\boldsymbol{x}}) \right] \tag{26}$$

and the functional measure $\mathcal{D}[\boldsymbol{x}(t)]$ is given by

$$\mathcal{D}[\boldsymbol{x}(t)] = \lim_{\epsilon\to 0} \epsilon^m \left( \frac{\det \boldsymbol{M}}{\sqrt{(2\pi\epsilon^3)^m \det \boldsymbol{S}_{\boldsymbol{w}}}} \right)^{L+1} \prod_{l=2}^{L}\prod_{j=1}^{m} \mathrm{d}x_{jl} \tag{27}$$

### 2.2. Functional series expansion and most probable path

The analytical evaluation of the WPI of Eq. (24) for determining the joint transition PDF $p\left(\boldsymbol{x}_f, \dot{\boldsymbol{x}}_f, t_f | \boldsymbol{x}_i, \dot{\boldsymbol{x}}_i, t_i\right)$ is not feasible in general, and thus, an approximate solution treatment is typically adopted (e.g., [17, 23]). In this regard, expressing $\boldsymbol{x}(t)$ as

$$\boldsymbol{x}(t) = \boldsymbol{x}_c(t) + \boldsymbol{X}(t) \tag{28}$$

and employing a Taylor-kind series expansion for the stochastic action $\mathcal{S}[\boldsymbol{x}, \dot{\boldsymbol{x}}, \ddot{\boldsymbol{x}}]$ (denoted in the following as $\mathcal{S}[\boldsymbol{x}]$ for simplicity) yields

$$\mathcal{S}[\boldsymbol{x}] = \mathcal{S}\left[\boldsymbol{x}_c + \boldsymbol{X}\right] = \mathcal{S}[\boldsymbol{x}_c] + \delta\mathcal{S}\left[\boldsymbol{x}_c, \boldsymbol{X}\right] + \frac{1}{2!}\delta^2\mathcal{S}\left[\boldsymbol{x}_c, \boldsymbol{X}\right] + \dots \tag{29}$$

In Eq. (28), $\boldsymbol{x}_c(t)$ is the most probable path associated with the maximum probability of occurrence $\mathcal{P}\left[\boldsymbol{x}_c(t)\right]$ and $\boldsymbol{X}(t)$ denotes the fluctuations around $\boldsymbol{x}_c(t)$ with $\boldsymbol{X}(t_i) = \boldsymbol{X}(t_f) = \dot{\boldsymbol{X}}(t_i) = \dot{\boldsymbol{X}}(t_f) = \mathbf{0}$. In Eq. (29), $\delta\mathcal{S}\left[\boldsymbol{x}_c, \boldsymbol{X}\right]$ represents the functional differential (or variation) of $\mathcal{S}$ evaluated on $\boldsymbol{x}_c(t)$. Considering Eq. (25), it takes the form

$$\delta\mathcal{S}\left[\boldsymbol{x}_c, \boldsymbol{X}\right] = \int_{t_i}^{t_f} \sum_{j=1}^{m} \left( \left.\frac{\partial\mathcal{L}}{\partial x_j}\right|_{x=x_c} X_j + \left.\frac{\partial\mathcal{L}}{\partial \dot{x}_j}\right|_{x=x_c} \dot{X}_j + \left.\frac{\partial\mathcal{L}}{\partial \ddot{x}_j}\right|_{x=x_c} \ddot{X}_j \right) \mathrm{d}t \tag{30}$$

Further, since maximum probability $\mathcal{P}\left[\boldsymbol{x}(t)\right]$ corresponds to minimum $\mathcal{S}\left[\boldsymbol{x}\right]$ based on Eq. (24), $\boldsymbol{x}_c(t)$ is associated with an extremum of the functional $\mathcal{S}\left[\boldsymbol{x}\right]$. In this context, calculus of variations dictates that the first variation of $\mathcal{S}\left[\boldsymbol{x}\right]$ vanishes for $\boldsymbol{x}(t) = \boldsymbol{x}_c(t)$, i.e.,

$$\delta\mathcal{S}\left[\boldsymbol{x}_c, \boldsymbol{X}\right] = 0 \tag{31}$$

Therefore, Eq. (29) becomes

$$\mathcal{S}\left[\boldsymbol{x}\right] = \mathcal{S}[\boldsymbol{x}_c] + \frac{1}{2!}\delta^2\mathcal{S}\left[\boldsymbol{x}_c, \boldsymbol{X}\right] + \dots \tag{32}$$

Furthermore, combining Eq. (30) and the extremality condition of Eq. (31) leads to

$$\int_{t_i}^{t_f} \left( \left.\frac{\partial\mathcal{L}}{\partial x_j}\right|_{x=x_c} X_j + \left.\frac{\partial\mathcal{L}}{\partial \dot{x}_j}\right|_{x=x_c} \frac{\mathrm{d}}{\mathrm{d}t} X_j + \left.\frac{\partial\mathcal{L}}{\partial \ddot{x}_j}\right|_{x=x_c} \frac{\mathrm{d}^2}{\mathrm{d}t^2} X_j \right) \mathrm{d}t = 0, \tag{33}$$

for $j = 1, \dots, m$

Next, integrating Eq. (33) by parts yields the system of Euler–Lagrange (EL) equations (e.g., [31])

$$\frac{\partial\mathcal{L}}{\partial x_{c,j}} - \frac{\mathrm{d}}{\mathrm{d}t}\frac{\partial\mathcal{L}}{\partial \dot{x}_{c,j}} + \frac{\mathrm{d}^2}{\mathrm{d}t^2}\frac{\partial\mathcal{L}}{\partial \ddot{x}_{c,j}} = 0, \quad \text{for } j = 1, \dots, m \tag{34}$$

in conjunction with the $4 \times m$ boundary conditions

$$\begin{cases} x_{c,j}(t_i) = x_{i,j} \\ x_{c,j}(t_f) = x_{f,j} \\ \dot{x}_{c,j}(t_i) = \dot{x}_{i,j} \\ \dot{x}_{c,j}(t_f) = \dot{x}_{f,j} \end{cases}, \quad \text{for } j = 1, \dots, m \tag{35}$$

where the most probable path is expressed as $\boldsymbol{x}_c(t) = \left[x_{c,j}(t)\right]_{m\times 1}$, and the boundary conditions as $\boldsymbol{x}_i = \left[x_{i,j}\right]_{m\times 1}$, $\boldsymbol{x}_f = \left[x_{f,j}\right]_{m\times 1}$, $\dot{\boldsymbol{x}}_i = \left[\dot{x}_{i,j}\right]_{m\times 1}$, and $\dot{\boldsymbol{x}}_f = \left[\dot{x}_{f,j}\right]_{m\times 1}$. The system of Eqs. (34)–(35) represents a deterministic nonlinear boundary value problem (BVP), which can be solved by standard numerical solution approaches such as Rayleigh–Ritz schemes (e.g., [15,20]).

Further, following solution of Eqs. (34)–(35) and determination of $\boldsymbol{x}_c(t)$, the expansion of Eq. (32) is evaluated approximately as

$$\mathcal{S}[\boldsymbol{x}] = \mathcal{S}[\boldsymbol{x}_c] + \log(C(t_f)^{-1}) \tag{36}$$

where the terms involving higher than second variations are treated collectively as a single constant $C(t_f)$. Substituting Eq. (36) into Eq. (24) yields an approximation for the response transition PDF in the form

$$p(\boldsymbol{x}_f, \dot{\boldsymbol{x}}_f, t_f | \boldsymbol{x}_i, \dot{\boldsymbol{x}}_i, t_i) \approx C(t_f)\ \exp\left(-\mathcal{S}\left[\boldsymbol{x}_c, \dot{\boldsymbol{x}}_c, \ddot{\boldsymbol{x}}_c\right]\right) \tag{37}$$

where $C(t_f)$ is evaluated by the normalization condition

$$\int_{-\infty}^{\infty}\int_{-\infty}^{\infty} p(\boldsymbol{x}_f, \dot{\boldsymbol{x}}_f, t_f | \boldsymbol{x}_i, \dot{\boldsymbol{x}}_i, t_i) \mathrm{d}\boldsymbol{x}_f \mathrm{d}\dot{\boldsymbol{x}}_f = 1 \tag{38}$$

It is remarked that Kougioumtzoglou and co-workers have developed various solution techniques based on the most probable path approximation of Eq. (37) for treating diverse problems in stochastic engineering dynamics. In fact, the most probable path approximation has demonstrated a satisfactory degree of accuracy in determining the stochastic response of various structural and mechanical nonlinear systems (e.g., [18,20,21,23]). In this regard, note that for linear systems, i.e., $\boldsymbol{g}(\boldsymbol{x}, \dot{\boldsymbol{x}}) = \mathbf{0}$ in Eq. (1), the most probable path approximation yields the exact joint response PDF as proved in [27].

Nevertheless, it was shown in [26] that accounting also for the second variation term in the functional series expansion of Eq. (32) yields an enhanced accuracy degree compared to the most probable path approximation. In this paper, and specifically in the following section, the quadratic WPI approximation technique developed in [26] for SDOF oscillators is generalized to account for MDOF systems.

## 3. A quadratic Wiener path integral approximation

In this section, a technique based on a quadratic WPI approximation is developed for determining the joint response transition PDF of nonlinear oscillators subject to stochastic excitation. The technique can be construed as a generalization of the results in [26] to account for MDOF systems.

Specifically, it is shown that compared to the standard most probable path WPI approximation presented in Section 2.2, the quadratic approximation yields enhanced accuracy in evaluating the system response joint PDF. This is primarily due to the fact that fluctuations around the most probable path are also accounted for by introducing a localized state-dependent factor in the approximate evaluation of the WPI. Further, a significant advantage of the enhancement relates to structural reliability assessment, and to the fact that the required in the most probable path approach PDF normalization step of Eq. (38) is circumvented. Thus, probabilities of rare events (e.g., failures) can be determined in a direct manner without the need for obtaining the complete joint response PDF first.

### 3.1. Accounting for the second variation term in the functional series expansion

Compared to the most probable path approximation described in Section 2.2, where only the first term is considered in the expansion of Eq. (32), both the first and the second variation terms are accounted for in the ensuing analysis. In this regard, Eq. (32) becomes

$$\mathcal{S}\left[\boldsymbol{x}\right] = \mathcal{S}[\boldsymbol{x}_c] + \frac{1}{2!}\delta^2\mathcal{S}\left[\boldsymbol{x}_c, \boldsymbol{X}\right] \tag{39}$$

Next, substituting Eq. (39) into Eq. (24), the joint response transition PDF is approximated as

$$p(\boldsymbol{x}_f, \dot{\boldsymbol{x}}_f, t_f | \boldsymbol{x}_i, \dot{\boldsymbol{x}}_i, t_i) = \phi\left(\boldsymbol{x}_f, \dot{\boldsymbol{x}}_f, t_f | \boldsymbol{x}_i, \dot{\boldsymbol{x}}_i, t_i\right) \exp\left(-\mathcal{S}\left[\boldsymbol{x}_c, \dot{\boldsymbol{x}}_c, \ddot{\boldsymbol{x}}_c\right]\right) \tag{40}$$

In Eq. (40), $\phi\left(\boldsymbol{x}_f, \dot{\boldsymbol{x}}_f, t_f | \boldsymbol{x}_i, \dot{\boldsymbol{x}}_i, t_i\right)$ represents a fluctuation factor expressed as

$$\phi\left(\boldsymbol{x}_f, \dot{\boldsymbol{x}}_f, t_f | \boldsymbol{x}_i, \dot{\boldsymbol{x}}_i, t_i\right) = \int_{\mathcal{C}\{\boldsymbol{x}_f, \dot{\boldsymbol{x}}_f, t_f; \boldsymbol{x}_i, \dot{\boldsymbol{x}}_i, t_i\}} \exp\left(-\frac{1}{2}\delta^2\mathcal{S}\left[\boldsymbol{x}_c, \boldsymbol{X}\right]\right) \mathcal{D}[\boldsymbol{X}(t)] \tag{41}$$

where $\mathcal{D}[\boldsymbol{X}(t)]$ is given by Eq. (27) and, considering the relationship of Eq. (25), the second variation $\delta^2\mathcal{S}\left[\boldsymbol{x}_c, \boldsymbol{X}\right]$ in Eq. (41) takes the form (e.g., [31])

$$\begin{aligned} \delta^2\mathcal{S}\left[\boldsymbol{x}_c, \boldsymbol{X}\right] = \int_{t_i}^{t_f} \sum_{j_1=1}^{m}\sum_{j_2=1}^{m} \Bigg( & \left.\frac{\partial^2\mathcal{L}}{\partial \ddot{x}_{j_1}\ddot{x}_{j_2}}\right|_{x=x_c} \ddot{X}_{j_1}\ddot{X}_{j_2} + \left.\frac{\partial^2\mathcal{L}}{\partial \dot{x}_{j_1}\dot{x}_{j_2}}\right|_{x=x_c} \dot{X}_{j_1}\dot{X}_{j_2} \\ & + \left.\frac{\partial^2\mathcal{L}}{\partial x_{j_1}\partial x_{j_2}}\right|_{x=x_c} X_{j_1}X_{j_2} + 2\left.\frac{\partial^2\mathcal{L}}{\partial \ddot{x}_{j_1}\partial \dot{x}_{j_2}}\right|_{x=x_c} \ddot{X}_{j_1}\dot{X}_{j_2} \\ & + 2\left.\frac{\partial^2\mathcal{L}}{\partial \ddot{x}_{j_1}\partial x_{j_2}}\right|_{x=x_c} \ddot{X}_{j_1}X_{j_2} + 2\left.\frac{\partial^2\mathcal{L}}{\partial \dot{x}_{j_1}\partial x_{j_2}}\right|_{x=x_c} \dot{X}_{j_1}X_{j_2} \Bigg) \mathrm{d}t \end{aligned} \tag{42}$$

Eq. (42) can be written, equivalently, in a compact form as

$$\delta^2\mathcal{S}\left[\boldsymbol{x}_c, \boldsymbol{X}\right] = \sum_{k=1}^{6} \Delta_k \tag{43}$$

where $\boldsymbol{X} = [X_1, \dots, X_m]^T$ and the scalar quantities $\Delta_1, \dots, \Delta_6$ are defined as

$$\begin{cases} \Delta_1 = \int_{t_i}^{t_f} \ddot{\boldsymbol{X}}^T \boldsymbol{D}_1 \ddot{\boldsymbol{X}} \mathrm{d}t \\ \Delta_2 = \int_{t_i}^{t_f} \dot{\boldsymbol{X}}^T \boldsymbol{D}_2 \dot{\boldsymbol{X}} \mathrm{d}t \\ \Delta_3 = \int_{t_i}^{t_f} \boldsymbol{X}^T \boldsymbol{D}_3 \boldsymbol{X} \mathrm{d}t \\ \Delta_4 = \int_{t_i}^{t_f} \left( \ddot{\boldsymbol{X}}^T \boldsymbol{D}_4 \dot{\boldsymbol{X}} + \dot{\boldsymbol{X}}^T \boldsymbol{D}_4^T \ddot{\boldsymbol{X}} \right) \mathrm{d}t \\ \Delta_5 = \int_{t_i}^{t_f} \left( \ddot{\boldsymbol{X}}^T \boldsymbol{D}_5 \boldsymbol{X} + \boldsymbol{X}^T \boldsymbol{D}_5^T \ddot{\boldsymbol{X}} \right) \mathrm{d}t \\ \Delta_6 = \int_{t_i}^{t_f} \left( \dot{\boldsymbol{X}}^T \boldsymbol{D}_6 \boldsymbol{X} + \boldsymbol{X}^T \boldsymbol{D}_6^T \dot{\boldsymbol{X}} \right) \mathrm{d}t \end{cases} \tag{44}$$

with the matrices $\boldsymbol{D}_1, \dots, \boldsymbol{D}_6$ given by

$$\begin{cases} \boldsymbol{D}_1 = \dfrac{\partial^2 \mathcal{L}}{\partial \ddot{\boldsymbol{x}}^2}\Big|_{\boldsymbol{x}=\boldsymbol{x}_c}; \quad \boldsymbol{D}_2 = \dfrac{\partial^2 \mathcal{L}}{\partial \dot{\boldsymbol{x}}^2}\Big|_{\boldsymbol{x}=\boldsymbol{x}_c}; \quad \boldsymbol{D}_3 = \dfrac{\partial^2 \mathcal{L}}{\partial \boldsymbol{x}^2}\Big|_{\boldsymbol{x}=\boldsymbol{x}_c} \\ \boldsymbol{D}_4 = \dfrac{\partial^2 \mathcal{L}}{\partial \ddot{\boldsymbol{x}} \partial \dot{\boldsymbol{x}}}\Big|_{\boldsymbol{x}=\boldsymbol{x}_c}; \quad \boldsymbol{D}_5 = \dfrac{\partial^2 \mathcal{L}}{\partial \ddot{\boldsymbol{x}} \partial \boldsymbol{x}}\Big|_{\boldsymbol{x}=\boldsymbol{x}_c}; \quad \boldsymbol{D}_6 = \dfrac{\partial^2 \mathcal{L}}{\partial \dot{\boldsymbol{x}} \partial \boldsymbol{x}}\Big|_{\boldsymbol{x}=\boldsymbol{x}_c} \end{cases} \tag{45}$$

Further, note that $\boldsymbol{D}_1$, $\boldsymbol{D}_2$, and $\boldsymbol{D}_3$ are symmetric. In this regard, considering the Lagrangian functional of Eq. (26) the first-order derivatives of $\mathcal{L}[\boldsymbol{x}, \dot{\boldsymbol{x}}, \ddot{\boldsymbol{x}}]$ with respect to $\boldsymbol{x}$, $\dot{\boldsymbol{x}}$, and $\ddot{\boldsymbol{x}}$ become

$$\begin{cases} \dfrac{\partial \mathcal{L}}{\partial \ddot{\boldsymbol{x}}} = \boldsymbol{M}^T \boldsymbol{S}_{\boldsymbol{w}}^{-1} [\boldsymbol{M}\ddot{\boldsymbol{x}} + \boldsymbol{C}\dot{\boldsymbol{x}} + \boldsymbol{K}\boldsymbol{x} + \boldsymbol{g}(\boldsymbol{x}, \dot{\boldsymbol{x}})] \\ \dfrac{\partial \mathcal{L}}{\partial \dot{\boldsymbol{x}}} = \left( \boldsymbol{C}^T + \dfrac{\partial \boldsymbol{g}}{\partial \dot{\boldsymbol{x}}} \right) \boldsymbol{S}_{\boldsymbol{w}}^{-1} [\boldsymbol{M}\ddot{\boldsymbol{x}} + \boldsymbol{C}\dot{\boldsymbol{x}} + \boldsymbol{K}\boldsymbol{x} + \boldsymbol{g}(\boldsymbol{x}, \dot{\boldsymbol{x}})] \\ \dfrac{\partial \mathcal{L}}{\partial \boldsymbol{x}} = \left( \boldsymbol{K}^T + \dfrac{\partial \boldsymbol{g}}{\partial \boldsymbol{x}} \right) \boldsymbol{S}_{\boldsymbol{w}}^{-1} [\boldsymbol{M}\ddot{\boldsymbol{x}} + \boldsymbol{C}\dot{\boldsymbol{x}} + \boldsymbol{K}\boldsymbol{x} + \boldsymbol{g}(\boldsymbol{x}, \dot{\boldsymbol{x}})] \end{cases} \tag{46}$$

respectively. Furthermore, the second-order derivatives of $\mathcal{L}[\boldsymbol{x}, \dot{\boldsymbol{x}}, \ddot{\boldsymbol{x}}]$ in Eq. (45) become

$$\begin{cases} \boldsymbol{D}_1 = \boldsymbol{M}^T \boldsymbol{S}_{\boldsymbol{w}}^{-1} \boldsymbol{M} \\ \boldsymbol{D}_2 = \left( \boldsymbol{C}^T + \dfrac{\partial \boldsymbol{g}}{\partial \dot{\boldsymbol{x}}} \right) \boldsymbol{S}_{\boldsymbol{w}}^{-1} \left( \boldsymbol{C}^T + \frac{\partial \boldsymbol{g}}{\partial \dot{\boldsymbol{x}}} \right)^T \Big|_{\boldsymbol{x}=\boldsymbol{x}_c} \\ \qquad + \displaystyle\sum_{j=1}^{m} \boldsymbol{s}_j [\boldsymbol{M}\ddot{\boldsymbol{x}} + \boldsymbol{C}\dot{\boldsymbol{x}} + \boldsymbol{K}\boldsymbol{x} + \boldsymbol{g}(\boldsymbol{x}, \dot{\boldsymbol{x}})] \dfrac{\partial^2 g_j}{\partial \dot{\boldsymbol{x}}^2}\Big|_{\boldsymbol{x}=\boldsymbol{x}_c} \\ \boldsymbol{D}_3 = \left( \boldsymbol{K}^T + \dfrac{\partial \boldsymbol{g}}{\partial \boldsymbol{x}} \right) \boldsymbol{S}_{\boldsymbol{w}}^{-1} \left( \boldsymbol{K}^T + \dfrac{\partial \boldsymbol{g}}{\partial \boldsymbol{x}} \right)^T \Big|_{\boldsymbol{x}=\boldsymbol{x}_c} \\ \qquad + \displaystyle\sum_{j=1}^{m} \boldsymbol{s}_j [\boldsymbol{M}\ddot{\boldsymbol{x}} + \boldsymbol{C}\dot{\boldsymbol{x}} + \boldsymbol{K}\boldsymbol{x} + \boldsymbol{g}(\boldsymbol{x}, \dot{\boldsymbol{x}})] \dfrac{\partial^2 g_j}{\partial \boldsymbol{x}^2}\Big|_{\boldsymbol{x}=\boldsymbol{x}_c} \\ \boldsymbol{D}_4 = \boldsymbol{C}^T \boldsymbol{S}_{\boldsymbol{w}}^{-1} \boldsymbol{M} + \dfrac{\partial \boldsymbol{g}}{\partial \dot{\boldsymbol{x}}} \boldsymbol{S}_{\boldsymbol{w}}^{-1} \boldsymbol{M}\Big|_{\boldsymbol{x}=\boldsymbol{x}_c} \\ \boldsymbol{D}_5 = \boldsymbol{K}^T \boldsymbol{S}_{\boldsymbol{w}}^{-1} \boldsymbol{M} + \dfrac{\partial \boldsymbol{g}}{\partial \boldsymbol{x}} \boldsymbol{S}_{\boldsymbol{w}}^{-1} \boldsymbol{M}\Big|_{\boldsymbol{x}=\boldsymbol{x}_c} \\ \boldsymbol{D}_6 = \left( \boldsymbol{K}^T + \frac{\partial \boldsymbol{g}}{\partial \boldsymbol{x}} \right) \boldsymbol{S}_{\boldsymbol{w}}^{-1} \left( \boldsymbol{C}^T + \frac{\partial \boldsymbol{g}}{\partial \dot{\boldsymbol{x}}} \right)^T \Big|_{\boldsymbol{x}=\boldsymbol{x}_c} \\ \qquad + \displaystyle\sum_{j=1}^{m} \boldsymbol{s}_j [\boldsymbol{M}\ddot{\boldsymbol{x}} + \boldsymbol{C}\dot{\boldsymbol{x}} + \boldsymbol{K}\boldsymbol{x} + \boldsymbol{g}(\boldsymbol{x}, \dot{\boldsymbol{x}})] \dfrac{\partial^2 g_j}{\partial \dot{\boldsymbol{x}} \partial \boldsymbol{x}}\Big|_{\boldsymbol{x}=\boldsymbol{x}_c} \end{cases} \tag{47}$$

where $\boldsymbol{s}_j$ and $g_j$ represent the $j$th rows of $\boldsymbol{S}_{\boldsymbol{w}}^{-1}$ and $\boldsymbol{g}$, respectively.

It is noted that the fluctuation factor $\phi\left(\boldsymbol{x}_f, \dot{\boldsymbol{x}}_f, t_f | \boldsymbol{x}_i, \dot{\boldsymbol{x}}_i, t_i\right)$ is expressed in Eq. (41) as a path integral with respect to paths $\boldsymbol{X}(t)$ with boundary conditions $\boldsymbol{X}(t_i) = \dot{\boldsymbol{X}}(t_i) = \boldsymbol{X}(t_f) = \dot{\boldsymbol{X}}(t_f) = \boldsymbol{0}$. Although the analytical calculation of an arbitrary path integral is, in general, a highly challenging task, a closed form expression is derived in the next section that facilitates the efficient calculation of $\phi\left(\boldsymbol{x}_f, \dot{\boldsymbol{x}}_f, t_f | \boldsymbol{x}_i, \dot{\boldsymbol{x}}_i, t_i\right)$.

Further, it is remarked that the fluctuation factor $\phi\left(\boldsymbol{x}_f, \dot{\boldsymbol{x}}_f, t_f | \boldsymbol{x}_i, \dot{\boldsymbol{x}}_i, t_i\right)$ is treated under the most probable path approximation as a single constant $C(t_f)$, dependent only on the final time instant $t_f$; see Eq. (37). In other words, it is considered independent of the final states $\{\boldsymbol{x}_f, \dot{\boldsymbol{x}}_f\}$. In contrast, based on the herein proposed quadratic approximation, $\phi\left(\boldsymbol{x}_f, \dot{\boldsymbol{x}}_f, t_f | \boldsymbol{x}_i, \dot{\boldsymbol{x}}_i, t_i\right)$ is expressed as a path integral in Eq. (41), dependent on the final state $\{\boldsymbol{x}_f, \dot{\boldsymbol{x}}_f\}$ through the most probable path $\boldsymbol{x}_c(t)$. This localization property of the state-dependent factor is expected to enhance the accuracy degree of the WPI technique compared to the standard most probable path approximation.

Furthermore, a significant advantage of the quadratic approximation relates to considerable reduction of the computational cost associated with reliability assessment applications. Specifically, calculating probabilities of rare events (e.g., structural failures) is associated with numerical integration of the joint response PDF over a relatively small domain, typically corresponding to the PDF tails. To this aim, applying the WPI technique based on the most probable path requires, first, the calculation of the joint PDF over its entire domain, followed next by the normalization step of Eq. (38). In contrast, the normalization step is circumvented in the WPI technique based on the quadratic approximation. In fact, the relatively few PDF points corresponding to the specific domain of interest related to the low probability event are determined directly based on Eq. (40); see also [26] for more details.

### 3.2. A closed form expression for efficient calculation of the fluctuation factor

Consider a discrete approximation of $\Delta_1, \dots, \Delta_6$ converging to Eq. (44) for $L \to \infty$. This is given by

$$\begin{cases} \Delta_1 = \displaystyle\sum_{l=0}^{L} \ddot{\boldsymbol{X}}_l^T \boldsymbol{D}_1 \ddot{\boldsymbol{X}}_l \epsilon \\ \Delta_2 = \displaystyle\sum_{l=0}^{L} \dot{\boldsymbol{X}}_l^T \boldsymbol{D}_{2l} \dot{\boldsymbol{X}}_l \epsilon \\ \Delta_3 = \displaystyle\sum_{l=0}^{L} \boldsymbol{X}_l^T \boldsymbol{D}_{3l} \boldsymbol{X}_l \epsilon \\ \Delta_4 = \displaystyle\sum_{l=0}^{L} \ddot{\boldsymbol{X}}_l^T \boldsymbol{D}_{4l} \dot{\boldsymbol{X}}_l \epsilon + \dot{\boldsymbol{X}}_l^T \boldsymbol{D}_{4l}^T \ddot{\boldsymbol{X}}_l \epsilon \\ \Delta_5 = \displaystyle\sum_{l=0}^{L} \ddot{\boldsymbol{X}}_l^T \boldsymbol{D}_{5l} \boldsymbol{X}_l \epsilon + \boldsymbol{X}_l^T \boldsymbol{D}_{5l}^T \ddot{\boldsymbol{X}}_l \epsilon \\ \Delta_6 = \displaystyle\sum_{l=0}^{L} \dot{\boldsymbol{X}}_l^T \boldsymbol{D}_{6l} \boldsymbol{X}_l \epsilon + \boldsymbol{X}_l^T \boldsymbol{D}_{6l}^T \dot{\boldsymbol{X}}_l \epsilon \end{cases} \tag{48}$$

where $\boldsymbol{X}_l = \boldsymbol{X}(t_l)$ and $\boldsymbol{D}_{kl} = \boldsymbol{D}_k(t_l)$, for $l \in \{0, \dots, L+1\}$ and $k \in \{1, \dots, 6\}$, and

$$\dot{\boldsymbol{X}}_l = \frac{\boldsymbol{X}_{l+1} - \boldsymbol{X}_l}{\epsilon}; \quad \ddot{\boldsymbol{X}}_l = \frac{\boldsymbol{X}_{l+2} - 2\boldsymbol{X}_{l+1} + \boldsymbol{X}_l}{\epsilon^2} \tag{49}$$

Combining Eq. (49) and $\boldsymbol{X}(t_i) = \boldsymbol{X}(t_f) = \dot{\boldsymbol{X}}(t_i) = \dot{\boldsymbol{X}}(t_f) = \boldsymbol{0}$ yields

$$\boldsymbol{X}_0 = \boldsymbol{X}_1 = \boldsymbol{X}_{L+1} = \boldsymbol{X}_{L+2} = \boldsymbol{0} \tag{50}$$

Next, substituting Eqs. (49)–(50) into Eq. (48) and manipulating, each and every term in the summations exhibits a quadratic form; that is, it constitutes a polynomial with all its terms of degree two (e.g., [32]). Further, Eq. (48) can be expressed in a more compact form as

$$\begin{cases} \Delta_1 = \boldsymbol{Y}^T \left[\mathbb{B}_0 \mathbb{B}_1\right] \boldsymbol{Y} \\ \Delta_2 = \boldsymbol{Y}^T \left[\mathbb{B}_0 \mathbb{B}_2\right] \boldsymbol{Y} \\ \Delta_3 = \boldsymbol{Y}^T \left[\mathbb{B}_0 \mathbb{B}_3\right] \boldsymbol{Y} \\ \Delta_4 = \boldsymbol{Y}^T \left[\mathbb{B}_0 \mathbb{B}_4\right] \boldsymbol{Y} \\ \Delta_5 = \boldsymbol{Y}^T \left[\mathbb{B}_0 \mathbb{B}_5\right] \boldsymbol{Y} \\ \Delta_6 = \boldsymbol{Y}^T \left[\mathbb{B}_0 \mathbb{B}_6\right] \boldsymbol{Y} \end{cases} \tag{51}$$

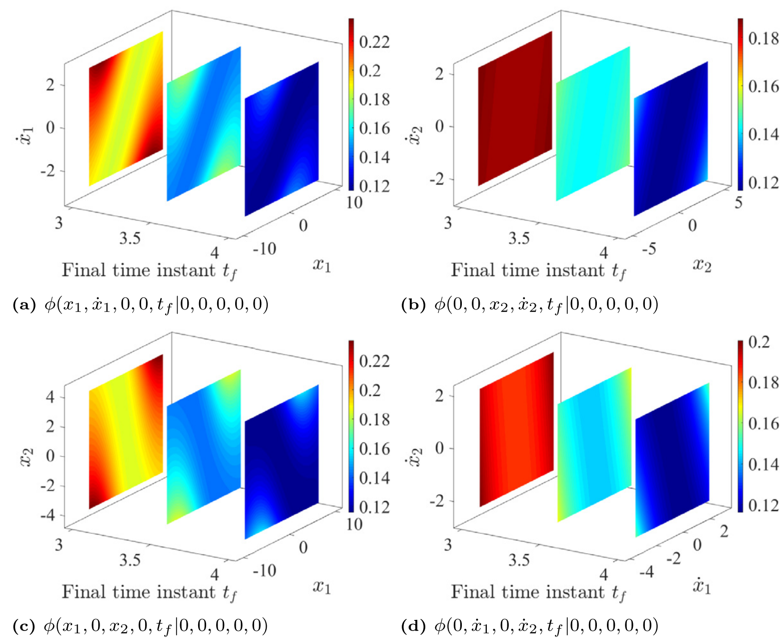


**Fig. 1.** Indicative fluctuation factor values determined by Eq. (61) for various time instants $t_f$; results corresponding to a stochastically excited 2-DOF nonlinear oscillator, whose dynamics is governed by Eq. (1) with $\boldsymbol{M} = m_0 \boldsymbol{I}_{2\times 2}$, $\boldsymbol{C} = c_0 \boldsymbol{Q}$, $\boldsymbol{K} = k_0 \boldsymbol{Q}$, $\boldsymbol{g}(\boldsymbol{x}, \dot{\boldsymbol{x}}) = \left[\epsilon_1 k_0 x_1^3, 0\right]^T$, $\boldsymbol{S_w} = 2\pi S_0 \boldsymbol{I}_{2\times 2}$, and parameter values ($m_0 = 1$; $c_0 = 0.35$; $k_0 = 0.5$; $\epsilon_1 = 0.1$; $S_0 = 0.0637$).

where $\boldsymbol{Y} = [\boldsymbol{X}_2, \ldots, \boldsymbol{X}_L]^T$ and the symmetric matrices $\mathbb{B}_0$, $\mathbb{B}_1$, …, $\mathbb{B}_6$ are provided in the Appendix.

Next, $\mathbb{A}$ is defined as

$$\mathbb{A} = \sum_{k=1}^{6} \mathbb{B}_k \tag{52}$$

and $\widetilde{\mathbb{A}}$ as

$$\widetilde{\mathbb{A}} = \mathbb{B}_0 \mathbb{A} \tag{53}$$

Note that both $\mathbb{A}$ and $\widetilde{\mathbb{A}}$ are symmetric, and taking into account Eq. (51), the second variation $\delta^2 \mathcal{S}\left[\boldsymbol{x}_c, \boldsymbol{X}\right]$ of Eq. (43) is expressed as

$$\delta^2 \mathcal{S}\left[\boldsymbol{x}_c, \boldsymbol{X}\right] = \sum_{q_1=1}^{m(L-1)} \sum_{q_2=1}^{m(L-1)} Y_{q_1} \widetilde{\mathbb{A}}_{q_1 q_2} Y_{q_2} = \boldsymbol{Y}^T \widetilde{\mathbb{A}} \boldsymbol{Y} \tag{54}$$

Finally, substituting Eq. (54) into Eq. (41), and considering a discrete-form path integral similar to Eq. (18), yields

$$\phi\left(\boldsymbol{x}_f, \dot{\boldsymbol{x}}_f, t_f | \boldsymbol{x}_i, \dot{\boldsymbol{x}}_i, t_i\right) = \lim_{\epsilon \to 0} \left\{ \epsilon^m \left[ \frac{\det \boldsymbol{M}}{\sqrt{\left(2\pi\epsilon^3\right)^m \det \boldsymbol{S_w}}} \right]^{L+1} \right.$$
$$\left. \times \int_{-\infty}^{\infty} \cdots \int_{-\infty}^{\infty} \exp\left( -\frac{1}{2} \sum_{q_1=1}^{m(L-1)} \sum_{q_2=1}^{m(L-1)} Y_{q_1} \widetilde{\mathbb{A}}_{q_1 q_2} Y_{q_2} \right) \mathrm{d}Y_1 \ldots \mathrm{d}Y_{m(L-1)} \right\} \tag{55}$$

Note that Eq. (55) represents a multi-dimensional Gaussian integral which can be calculated analytically as (e.g., [17])

$$\int_{-\infty}^{\infty} \cdots \int_{-\infty}^{\infty} \exp\left( -\frac{1}{2} \sum_{q_1=1}^{m(L-1)} \sum_{q_2=1}^{m(L-1)} Y_{q_1} \widetilde{\mathbb{A}}_{q_1 q_2} Y_{q_2} \right) \mathrm{d}Y_1 \ldots \mathrm{d}Y_{m(L-1)} = \sqrt{\frac{(2\pi)^{m(L-1)}}{\det \widetilde{\mathbb{A}}}} \tag{56}$$

where $\det \widetilde{\mathbb{A}}$ is given by

$$\det \widetilde{\mathbb{A}} = (\det \mathbb{B}_0)(\det \mathbb{A}) = \left[ \frac{(\det \boldsymbol{M})^2}{\epsilon^{3m} \det \boldsymbol{S_w}} \right]^{L-1} (\det \mathbb{A}) \tag{57}$$

Substituting Eqs. (56)–(57) into Eq. (55), yields

$$\phi\left(\boldsymbol{x}_f, \dot{\boldsymbol{x}}_f, t_f | \boldsymbol{x}_i, \dot{\boldsymbol{x}}_i, t_i\right) = \lim_{\epsilon \to 0} \frac{(\det \boldsymbol{M})^2}{\left(2\pi\epsilon^2\right)^m \det \boldsymbol{S_w} \sqrt{\det \mathbb{A}}} \tag{58}$$

### 3.3. Mechanization of the technique

The numerical implementation of the developed technique comprises the following steps:

(i) For a given time instant $t_f$, consider an effective domain of final states $\{\boldsymbol{x}_f, \dot{\boldsymbol{x}}_f\}$ and discretize it into $N_s^{2m}$ points, where $2m$ is the number of stochastic dimensions ($m$ displacements and $m$ velocities).
(ii) For each final state $\{\boldsymbol{x}_f, \dot{\boldsymbol{x}}_f\}$ determine the most probable path $\boldsymbol{x}_c(t)$ by solving the BVP problem of Eqs. (34)–(35).
(iii) Evaluate the parameter matrices $\mathbb{B}_1, \ldots, \mathbb{B}_6$ based on the Appendix, where $L = 1000$ is an indicative value.
(iv) Compute the determinant of $\mathbb{A}$ and evaluate the fluctuation factor $\phi\left(\boldsymbol{x}_f, \dot{\boldsymbol{x}}_f, t_f | \boldsymbol{x}_i, \dot{\boldsymbol{x}}_i, t_i\right)$ by Eq. (58).
(v) Obtain a specific point of the joint transition PDF $p(\boldsymbol{x}_f, \dot{\boldsymbol{x}}_f, t_f | \boldsymbol{x}_i, \dot{\boldsymbol{x}}_i, t_i)$ by employing Eq. (40).
(vi) Repeat steps (ii)–(v) for all $N_s^{2m}$ points to determine the complete joint response PDF $p(\boldsymbol{x}_f, \dot{\boldsymbol{x}}_f, t_f | \boldsymbol{x}_i, \dot{\boldsymbol{x}}_i, t_i)$.

Clearly, compared with the most probable path approximation, the enhanced accuracy of the quadratic approximation technique comes at the expense of some added modest computational cost due to the calculation of $\det \mathbb{A}$ in the definition of the fluctuation factor. Further, the exhibited computational efficiency can be readily enhanced by replacing step (i) with recently developed solution schemes based on compressive sampling concepts (e.g., [24,33]) that require the consideration of only few final states $\{\boldsymbol{x}_f, \dot{\boldsymbol{x}}_f\}$; see also [25] for a broad perspective.

## 4. Numerical examples

To demonstrate the reliability of the quadratic WPI approximation, three distinct numerical examples are considered in this section pertaining to 2-DOF systems exhibiting diverse nonlinear behaviors. Their dynamics is governed by Eq. (1) with $\boldsymbol{M} = m_0 \boldsymbol{I}_{2\times 2}$, $\boldsymbol{S_w} = 2\pi S_0 \boldsymbol{I}_{2\times 2}$, $\boldsymbol{C} = c_0 \boldsymbol{Q}$, and $\boldsymbol{K} = k_0 \boldsymbol{Q}$, where

$$\boldsymbol{Q} = \begin{bmatrix} 1 & -1 \\ -1 & 2 \end{bmatrix} \tag{59}$$

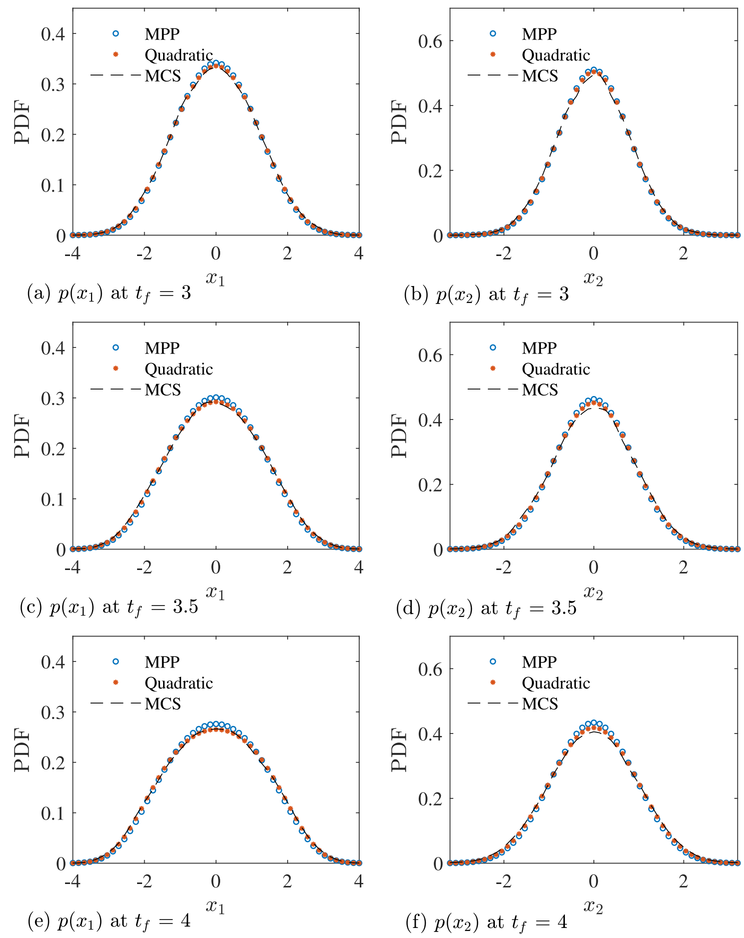


**Fig. 2.** Marginal response PDFs of a stochastically excited 2-DOF nonlinear oscillator, whose dynamics is governed by Eq. (1) with $\boldsymbol{M} = m_0\boldsymbol{I}_{2\times2}$, $\boldsymbol{C} = c_0\boldsymbol{Q}$, $\boldsymbol{K} = k_0\boldsymbol{Q}$, $\boldsymbol{g}(\boldsymbol{x},\dot{\boldsymbol{x}}) = \left[\epsilon_1 k_0 x_1^3, 0\right]^T$, $\boldsymbol{S_w} = 2\pi S_0 \boldsymbol{I}_{2\times2}$, and parameter values ($m_0 = 1$; $c_0 = 0.35$; $k_0 = 0.5$; $\epsilon_1 = 0.1$; $S_0 = 0.0637$); comparisons between results obtained by the most probable path (MPP) approximation (shown with blue circles), by the quadratic approximation (shown with red asterisks), and by pertinent MCS data (50,000 realizations; shown with black dashed line).

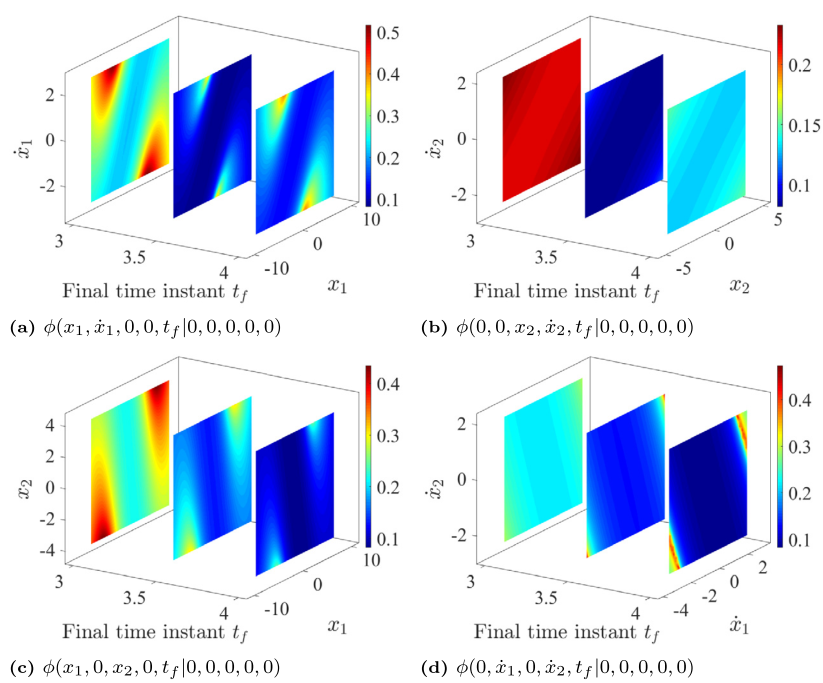


**Fig. 3.** Indicative fluctuation factor values determined by Eq. (61) for various time instants $t_f$; results corresponding to a stochastically excited 2-DOF nonlinear oscillator, whose dynamics is governed by Eq. (1) with $\boldsymbol{M} = m_0\boldsymbol{I}_{2\times2}$, $\boldsymbol{C} = c_0\boldsymbol{Q}$, $\boldsymbol{K} = k_0\boldsymbol{Q}$, $\boldsymbol{g}(\boldsymbol{x},\dot{\boldsymbol{x}}) = \left[\epsilon_1 k_0 x_1^3, 0\right]^T$, $\boldsymbol{S_w} = 2\pi S_0 \boldsymbol{I}_{2\times2}$, and parameter values ($m_0 = 1$; $c_0 = 1$; $k_0 = -0.5$; $\epsilon_1 = -0.5$; $S_0 = 0.0637$).

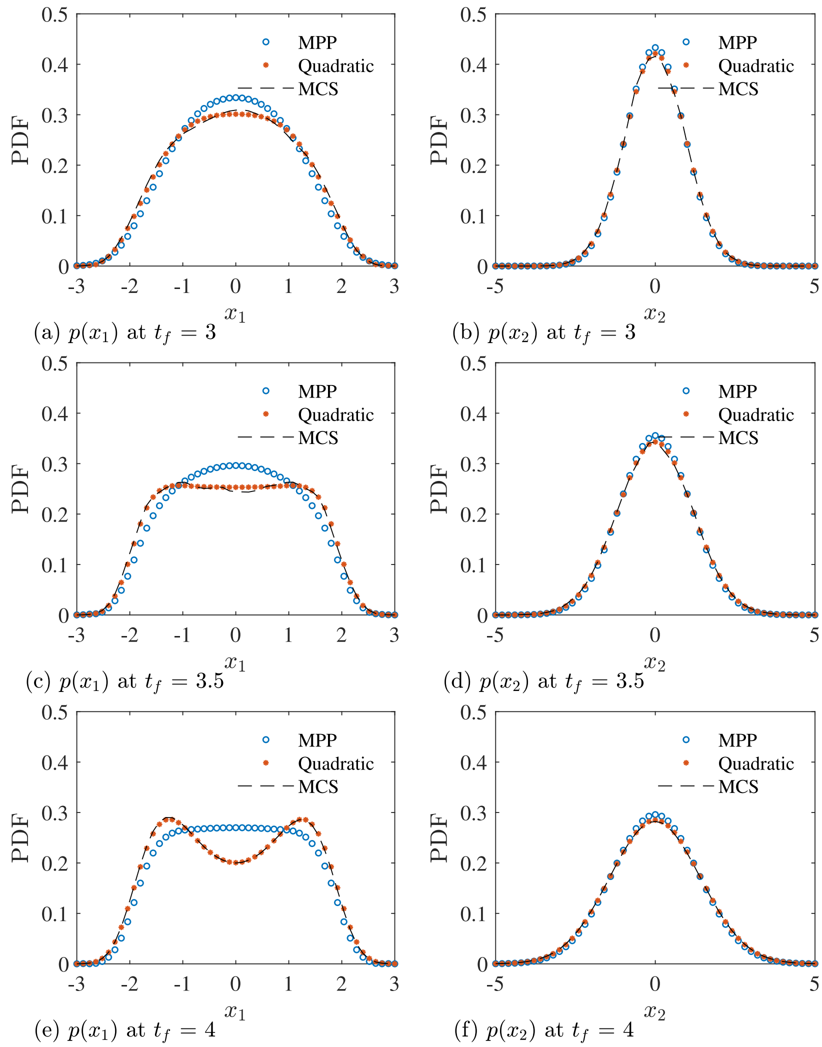


**Fig. 4.** Marginal response PDFs of a stochastically excited 2-DOF nonlinear oscillator, whose dynamics is governed by Eq. (1) with $\boldsymbol{M} = m_0 \boldsymbol{I}_{2\times2}$, $\boldsymbol{C} = c_0 \boldsymbol{Q}$, $\boldsymbol{K} = k_0 \boldsymbol{Q}$, $\boldsymbol{g}(\boldsymbol{x}, \dot{\boldsymbol{x}}) = \left[\epsilon_1 k_0 x_1^3, 0\right]^T$, $\boldsymbol{S}_w = 2\pi S_0 \boldsymbol{I}_{2\times2}$, and parameter values ($m_0 = 1$; $c_0 = 1$; $k_0 = -0.5$; $\epsilon_1 = -0.5$; $S_0 = 0.0637$); comparisons between results obtained by the most probable path (MPP) approximation (shown with blue circles), by the quadratic approximation (shown with red asterisks), and by pertinent MCS data (50,000 realizations; shown with black dashed line).

In this regard, $\boldsymbol{D}_1, \dots, \boldsymbol{D}_6$ of Eq. (47) become

$$\begin{cases} \boldsymbol{D}_1 = \dfrac{m_0^2}{2\pi S_0} \boldsymbol{I}_{2\times2} \\ \boldsymbol{D}_2 = \dfrac{1}{2\pi S_0} \left( c_0 \boldsymbol{Q} + \dfrac{\partial \boldsymbol{g}}{\partial \dot{\boldsymbol{x}}} \right) \left( c_0 \boldsymbol{Q} + \dfrac{\partial \boldsymbol{g}}{\partial \dot{\boldsymbol{x}}} \right)^T \Big|_{\boldsymbol{x}=\boldsymbol{x}_c} + \displaystyle\sum_{j=1}^{m} s_j \left[ m_0 \ddot{\boldsymbol{x}} + c_0 \boldsymbol{Q} \dot{\boldsymbol{x}} + k_0 \boldsymbol{Q} \boldsymbol{x} + \boldsymbol{g} \right] \dfrac{\partial^2 g_j}{\partial \dot{\boldsymbol{x}}^2} \Big|_{\boldsymbol{x}=\boldsymbol{x}_c} \\ \boldsymbol{D}_3 = \dfrac{1}{2\pi S_0} \left( k_0 \boldsymbol{Q} + \dfrac{\partial \boldsymbol{g}}{\partial \boldsymbol{x}} \right) \left( k_0 \boldsymbol{Q} + \dfrac{\partial \boldsymbol{g}}{\partial \boldsymbol{x}} \right)^T \Big|_{\boldsymbol{x}=\boldsymbol{x}_c} + \displaystyle\sum_{j=1}^{m} s_j \left[ m_0 \ddot{\boldsymbol{x}} + c_0 \boldsymbol{Q} \dot{\boldsymbol{x}} + k_0 \boldsymbol{Q} \boldsymbol{x} + \boldsymbol{g} \right] \dfrac{\partial^2 g_j}{\partial \boldsymbol{x}^2} \Big|_{\boldsymbol{x}=\boldsymbol{x}_c} \\ \boldsymbol{D}_4 = \dfrac{m_0}{2\pi S_0} \left( c_0 \boldsymbol{Q} + \dfrac{\partial \boldsymbol{g}}{\partial \dot{\boldsymbol{x}}} \right) \Big|_{\boldsymbol{x}=\boldsymbol{x}_c} \\ \boldsymbol{D}_5 = \dfrac{m_0}{2\pi S_0} \left( k_0 \boldsymbol{Q} + \dfrac{\partial \boldsymbol{g}}{\partial \boldsymbol{x}} \right) \Big|_{\boldsymbol{x}=\boldsymbol{x}_c} \\ \boldsymbol{D}_6 = \dfrac{1}{2\pi S_0} \left( k_0 \boldsymbol{Q} + \dfrac{\partial \boldsymbol{g}}{\partial \boldsymbol{x}} \right) \left( c_0 \boldsymbol{Q} + \dfrac{\partial \boldsymbol{g}}{\partial \dot{\boldsymbol{x}}} \right)^T \Big|_{\boldsymbol{x}=\boldsymbol{x}_c} + \displaystyle\sum_{j=1}^{m} s_j \left[ m_0 \ddot{\boldsymbol{x}} + c_0 \boldsymbol{Q} \dot{\boldsymbol{x}} + k_0 \boldsymbol{Q} \boldsymbol{x} + \boldsymbol{g} \right] \dfrac{\partial^2 g_j}{\partial \dot{\boldsymbol{x}} \partial \boldsymbol{x}} \Big|_{\boldsymbol{x}=\boldsymbol{x}_c} \end{cases} \tag{60}$$

Further, the expression for the fluctuation factor $\phi(\boldsymbol{x}_f, \dot{\boldsymbol{x}}_f, t_f | \boldsymbol{x}_i, \dot{\boldsymbol{x}}_i, t_i)$ in Eq. (58) degenerates to

$$\phi(\boldsymbol{x}_f, \dot{\boldsymbol{x}}_f, t_f | \boldsymbol{x}_i, \dot{\boldsymbol{x}}_i, t_i) = \lim_{\epsilon \to 0} \frac{m_0^4}{16\pi^4 S_0^2 \epsilon^4 \sqrt{\det \mathbb{A}}} \tag{61}$$

In the following examples, the value $N_s = 51$ is used for the discretization of the joint PDF effective domain. The results obtained by the WPI-based technique are compared with pertinent MCS-based data (50,000 realizations).

### 4.1. Cubic stiffness nonlinearities

Consider a 2-DOF nonlinear system with $\boldsymbol{g}(\boldsymbol{x}, \dot{\boldsymbol{x}}) = \left[\epsilon_1 k_0 x_1^3, 0\right]^T$ and parameter values $m_0 = 1$, $c_0 = 0.35$, $k_0 = 0.5$, $\epsilon_1 = 0.1$, and $S_0 = 0.0637$. The initial conditions are $t_i = 0$ and $\boldsymbol{x}_i = \dot{\boldsymbol{x}}_i = \boldsymbol{0}$.

Fig. 1 shows indicative fluctuation factor values corresponding to various final time instants $t_f$. Next, the joint transition PDF is obtained by Eq. (40) and indicative results are shown in Fig. 2 corresponding to the marginal PDFs $p(x_1)$ and $p(x_2)$. Clearly, as anticipated due to the localized nature of the state-dependent fluctuation factor in Eq. (40), it is shown in Fig. 2 that the quadratic approximation exhibits an enhanced accuracy degree compared to the most probable path scheme.

### 4.2. Nonlinear system with bimodal response PDF

Consider next a 2-DOF nonlinear system with $\boldsymbol{g}(\boldsymbol{x}, \dot{\boldsymbol{x}}) = \left[\epsilon_1 k_0 x_1^3, 0\right]^T$ and parameter values $m_0 = 1$, $c_0 = 1$, $k_0 = -0.5$, $\epsilon_1 = -0.5$, and $S_0 = 0.0637$. The initial conditions are $t_i = 0$ and $\boldsymbol{x}_i = \dot{\boldsymbol{x}}_i = \boldsymbol{0}$.

Further, Fig. 3 shows indicative fluctuation factor values obtained by Eq. (61). Furthermore, the marginal PDFs $p(x_1)$ and $p(x_2)$ are plotted

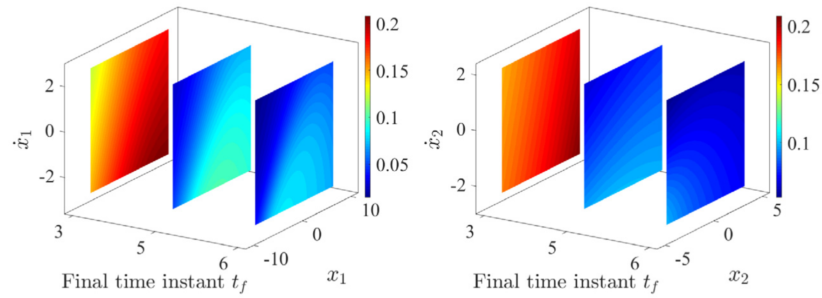


(a) $\phi(x_1, \dot{x}_1, 0, 0, t_f | 0, 0, 0, 0, 0)$ (b) $\phi(0, 0, x_2, \dot{x}_2, t_f | 0, 0, 0, 0, 0)$

(c) $\phi(x_1, 0, x_2, 0, t_f | 0, 0, 0, 0, 0)$ (d) $\phi(0, \dot{x}_1, 0, \dot{x}_2, t_f | 0, 0, 0, 0, 0)$

**Fig. 5.** Indicative fluctuation factor values determined by Eq. (61) for various time instants $t_f$; results corresponding to a stochastically excited 2-DOF nonlinear oscillator, whose dynamics is governed by Eq. (1) with $\boldsymbol{M} = m_0 \boldsymbol{I}_{2\times2}$, $\boldsymbol{C} = c_0 \boldsymbol{Q}$, $\boldsymbol{K} = k_0 \boldsymbol{Q}$, $\boldsymbol{g}(\boldsymbol{x}, \dot{\boldsymbol{x}}) = \left[\epsilon_1 k_0 x_1^2, 0\right]^T$, $\boldsymbol{S}_{\boldsymbol{w}} = 2\pi S_0 \boldsymbol{I}_{2\times2}$, and parameter values ($m_0 = 1$; $c_0 = 0.2$; $k_0 = 1$; $\epsilon_1 = 0.1$; $S_0 = 0.0637$).

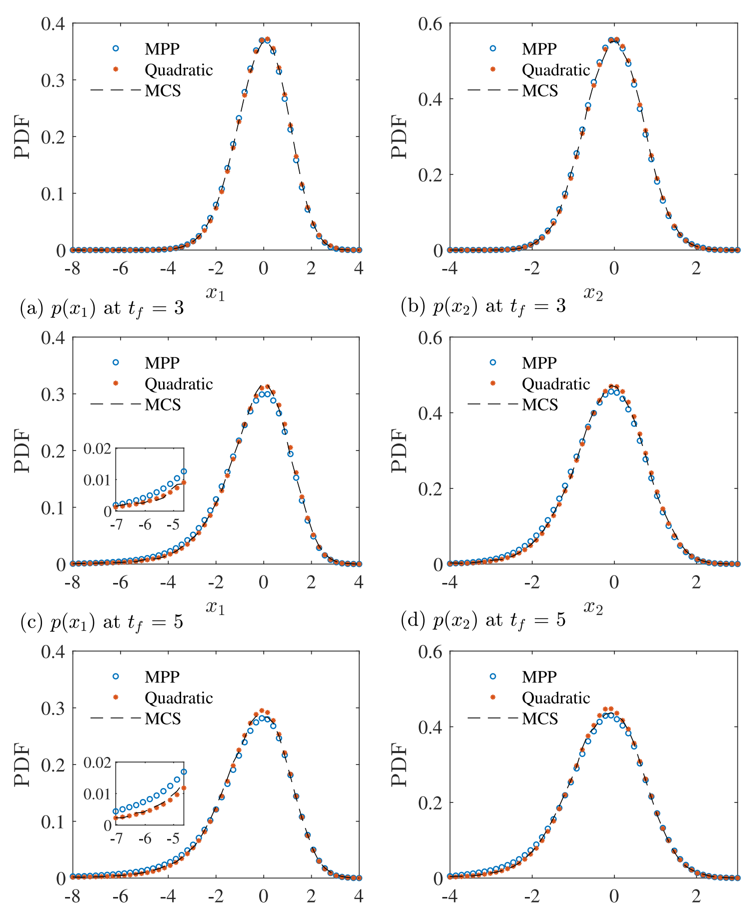


(a) $p(x_1)$ at $t_f = 3$ (b) $p(x_2)$ at $t_f = 3$

(c) $p(x_1)$ at $t_f = 5$ (d) $p(x_2)$ at $t_f = 5$

(e) $p(x_1)$ at $t_f = 6$ (f) $p(x_2)$ at $t_f = 6$

**Fig. 6.** Marginal response PDFs of a stochastically excited 2-DOF nonlinear oscillator, whose dynamics is governed by Eq. (1) with $\boldsymbol{M} = m_0 \boldsymbol{I}_{2\times2}$, $\boldsymbol{C} = c_0 \boldsymbol{Q}$, $\boldsymbol{K} = k_0 \boldsymbol{Q}$, $\boldsymbol{g}(\boldsymbol{x}, \dot{\boldsymbol{x}}) = \left[\epsilon_1 k_0 x_1^2, 0\right]^T$, $\boldsymbol{S}_{\boldsymbol{w}} = 2\pi S_0 \boldsymbol{I}_{2\times2}$, and parameter values ($m_0 = 1$; $c_0 = 0.2$; $k_0 = 1$; $\epsilon_1 = 0.1$; $S_0 = 0.0637$); comparisons between results obtained by the most probable path (MPP) approximation (shown with blue circles), by the quadratic approximation (shown with red asterisks), and by pertinent MCS data (50,000 realizations; shown with black dashed line).

in Fig. 4 for various final time instants. It is readily seen that the herein developed technique based on the quadratic WPI approximation outperforms the standard most probable path approach in terms of exhibited accuracy.

Note that this superior performance becomes more prevalent for larger time instants, where the marginal response displacement PDF $p(x_1)$ tends to become bimodal; see, for instance, Fig. 4(e). In fact, the most probable path approximation fails to capture the PDF bimodal characteristic, and yields a PDF estimate that exhibits a plateau of approximately constant value connecting the two modes. This is due to the fact that the joint PDF representation of Eq. (37) based on the most probable path attains a global maximum at $(\boldsymbol{x}_f, \dot{\boldsymbol{x}}_f) = (\mathbf{0}, \mathbf{0})$. This limitation is addressed in this paper by considering the state-dependent fluctuation factor whose impact on determining the joint response PDF via Eq. (40) leads to an enhanced accuracy degree and to capturing satisfactorily the bimodal shape as shown in Fig. 4(e).

### 4.3. Nonlinear system with asymmetric response PDF

Consider next a 2-DOF system with asymmetric nonlinearities governed by Eq. (1) with $\boldsymbol{g}(\boldsymbol{x}, \dot{\boldsymbol{x}}) = \left[\epsilon_1 k_0 x_1^2, 0\right]^T$ and parameter values $m_0 = 1$, $c_0 = 0.2$, $k_0 = 1$, $\epsilon_1 = 0.1$, and $S_0 = 0.0637$. The initial conditions are $t_i = 0$ and $\boldsymbol{x}_i = \dot{\boldsymbol{x}}_i = \mathbf{0}$.

In the following, indicative values of the fluctuation factor are computed and plotted in Fig. 5. Next, the joint response PDF is determined and the marginal PDFs $p(x_1)$ and $p(x_2)$ are plotted in Fig. 6 for arbitrarily chosen time instants. Comparisons with pertinent MCS-based estimates demonstrate increased accuracy of the quadratic approximation over the most probable path approach. This is further corroborated by focusing on the magnified subplots of Fig. 6(c) and (e) corresponding to the tails of the response PDF. It is readily seen that the accuracy degree of the WPI technique is significantly enhanced when the quadratic approximation is employed.

## 5. Concluding remarks

In this paper, a novel WPI technique has been developed for stochastic response determination of nonlinear dynamical systems. The technique can be construed as an extension of the results in [26] to account for MDOF systems. Specifically, the system response joint transition PDF has been expressed as a functional integral over the space of possible paths satisfying initial and final conditions in time. Next, a Taylor-kind series expansion has been employed for the functional integral and a quadratic approximation has been considered. Further, resorting to a variational principle has led to a functional optimization problem to be solved numerically for the most probable path. Furthermore, the most probable path has been used for evaluating the terms in the functional series expansion and for determining approximately the joint response PDF. Compared to the standard most probable path approach, where only the first term is retained in the WPI expansion, employing a quadratic approximation and accounting also for the second variation term yields an enhanced accuracy degree. This is due to the fact that a localized state-dependent factor is introduced in the approximate evaluation of the joint response PDF. Three illustrative numerical examples have been considered pertaining to oscillators with diverse nonlinear behaviors. Comparisons with MCS data have demonstrated the enhanced accuracy degree exhibited by the herein developed technique.

## Declaration of competing interest

The authors declare that they have no known competing financial interests or personal relationships that could have appeared to influence the work reported in this paper.

## Acknowledgments

I. A. Kougioumtzoglou gratefully acknowledges the support through his CAREER award by the CMMI Division of the National Science Foundation, United States (Award No. 1748537). Y. Zhao appreciates the financial support by the Zhejiang Province Public Welfare Technology Application Research Project, China (Grant No. LGG19F020005) and the National Natural Science Foundation of China (Grant No. 52106019).

## Appendix

The $m(L-1) \times m(L-1)$ symmetric matrix $\mathbb{B}_0$ is given by

$$\mathbb{B}_0 = \frac{1}{\epsilon^3}\begin{bmatrix} \boldsymbol{D}_1 & & \\ & \ddots & \\ & & \boldsymbol{D}_1 \end{bmatrix} \tag{A.1}$$

and the $m(L-1) \times m(L-1)$ symmetric matrices $\mathbb{B}_1, \ldots, \mathbb{B}_6$ are given by

$$\mathbb{B}_1 = \begin{bmatrix} 6\boldsymbol{I} & & & & & & symm \\ -4\boldsymbol{I} & 6\boldsymbol{I} & & & & & \\ \boldsymbol{I} & -4\boldsymbol{I} & 6\boldsymbol{I} & & & & \\ \mathbf{0} & \ddots & \ddots & \ddots & & & \\ \vdots & & & & 6\boldsymbol{I} & & \\ & & & & -4\boldsymbol{I} & 6\boldsymbol{I} & \\ \mathbf{0} & & \cdots & \mathbf{0} & \boldsymbol{I} & -4\boldsymbol{I} & 6\boldsymbol{I} \end{bmatrix} \tag{A.2}$$

$$\mathbb{B}_2 = \epsilon^2\begin{bmatrix} \boldsymbol{P}_2^1 + \boldsymbol{P}_2^2 & & & & symm \\ -\boldsymbol{P}_2^2 & \boldsymbol{P}_2^2 + \boldsymbol{P}_2^3 & & & \\ \mathbf{0} & \ddots & \ddots & & \\ \vdots & & & & \\ \mathbf{0} & \cdots & \mathbf{0} & -\boldsymbol{P}_2^{L-1} & \boldsymbol{P}_2^{L-1} + \boldsymbol{P}_2^L \end{bmatrix} \tag{A.3}$$

$$\mathbb{B}_3 = \epsilon^4\begin{bmatrix} \boldsymbol{P}_3^2 & & & symm \\ \mathbf{0} & \ddots & & \\ \vdots & & & \\ \mathbf{0} & \cdots & \mathbf{0} & \boldsymbol{P}_3^L \end{bmatrix} \tag{A.4}$$

$$\mathbb{B}_4 = \epsilon\begin{bmatrix} -4\boldsymbol{P}_4^1 - 2\boldsymbol{P}_4^2 & & & & & symm \\ \boldsymbol{P}_4^1 + 3\boldsymbol{P}_4^2 & \ddots & & & & \\ -\boldsymbol{P}_4^2 & \ddots & & & & \\ \mathbf{0} & \ddots & & & & \\ \vdots & & & & & \\ \mathbf{0} & \cdots & \mathbf{0} & -\boldsymbol{P}_4^{L-2} & \boldsymbol{P}_4^{L-2} + 3\boldsymbol{P}_4^{L-1} & -4\boldsymbol{P}_4^{L-1} - 2\boldsymbol{P}_4^L \end{bmatrix} \tag{A.5}$$

$$\mathbb{B}_5 = \epsilon^2\begin{bmatrix} 2\boldsymbol{P}_5^2 & & & & & symm \\ -2\boldsymbol{P}_5^2 & \ddots & & & & \\ \boldsymbol{P}_5^2 & \ddots & & & & \\ \mathbf{0} & \ddots & & & & \\ \vdots & & & & & \\ \mathbf{0} & \cdots & \mathbf{0} & \boldsymbol{P}_5^{L-2} & -2\boldsymbol{P}_5^{L-1} & 2\boldsymbol{P}_2^L \end{bmatrix} \tag{A.6}$$

and

$$\mathbb{B}_6 = \epsilon^3\begin{bmatrix} -2\boldsymbol{P}_6^2 & & & & symm \\ \boldsymbol{P}_6^2 & \ddots & & & \\ \mathbf{0} & \ddots & & & \\ \vdots & & & & \\ \mathbf{0} & \cdots & \mathbf{0} & \boldsymbol{P}_6^{L-1} & -2\boldsymbol{P}_6^L \end{bmatrix} \tag{A.7}$$

respectively, where $\boldsymbol{P}_k^l = \boldsymbol{P}_k(t_l)$ for $k \in \{2, \ldots, 6\}$, and $\boldsymbol{P}_k(t)$ are determined by

$$\begin{cases} \boldsymbol{P}_2 = \boldsymbol{D}_1^{-1}\boldsymbol{D}_2; \quad \boldsymbol{P}_3 = \boldsymbol{D}_1^{-1}\boldsymbol{D}_3 \quad \boldsymbol{P}_4 = \boldsymbol{D}_1^{-1}\boldsymbol{D}_4 \\ \boldsymbol{P}_5 = \boldsymbol{D}_1^{-1}\boldsymbol{D}_5; \quad \boldsymbol{P}_6 = \boldsymbol{D}_1^{-1}\boldsymbol{D}_6 \end{cases} \tag{A.8}$$

## References

[1] J.B. Roberts, P.D. Spanos, Random Vibration and Statistical Linearization, Dover, New York, 2003.
[2] J. Li, J. Chen, Stochastic Dynamics of Structures, Wiley, New York, 2009.
[3] M. Grigoriu, Stochastic Systems: Uncertainty Quantification and Propagation, Springer, Berlin, 2012.
[4] M.F. Wehner, W.G. Wolfer, Numerical evaluation of path-integral solutions to Fokker-Planck equations, Phys. Rev. A 27 (5) (1983) 2663–2670.
[5] M. Grigoriu, Applications of diffusion models to reliability analysis of Daniels systems, Struct. Saf. 7 (1990) 219–228.
[6] A. Naess, J. Johnsen, Response statistics of nonlinear, compliant offshore structures by the path integral solution method, Probab. Eng. Mech. 8 (1993) 91–106.
[7] L. Chen, E.R. Jakobsen, A. Naess, On numerical density approximations of solutions of SDEs with unbounded coefficients, Adv. Comput. Math. 44 (2018) 693–721.
[8] P. Alevras, D. Yurchenko, GPU computing for accelerating the numerical path integration approach, Comput. Struct. 171 (2016) 46–53.
[9] M. Di Paola, G. Alotta, Path integral methods for the probabilistic analysis of nonlinear systems under a white-noise process, ASCE-ASME J. Risk Uncertain. Eng. Syst. B: Mech. Eng. 6 (4) (2020) 040801.
[10] L. Socha, Linearization Methods for Stochastic Dynamic Systems, Springer, Berlin, 2007.
[11] I.A. Kougioumtzoglou, P.D. Spanos, Harmonic wavelets based response evolutionary power spectrum determination of linear and non-linear oscillators with fractional derivative elements, Int. J. Non-Linear Mech. 80 (2016) 66–75.
[12] V.C. Fragkoulis, I.A. Kougioumtzoglou, A.A. Pantelous, Statistical linearization of nonlinear structural systems with singular matrices, J. Eng. Mech. 142 (9) (2016) 04016063.
[13] I.A. Kougioumtzoglou, P.D. Spanos, An analytical Wiener path integral technique for non-stationary response determination of nonlinear oscillators, Probab. Eng. Mech. 28 (2012) 125–131.
[14] A. Di Matteo, I.A. Kougioumtzoglou, A. Pirrotta, P.D. Spanos, M. Di Paola, Stochastic response determination of nonlinear oscillators with fractional derivatives elements via the Wiener path integral, Probab. Eng. Mech. 38 (2014) 127–135.
[15] I.A. Kougioumtzoglou, A Wiener path integral solution treatment and effective material properties of a class of one-dimensional stochastic mechanics problems, J. Eng. Mech. 143 (6) (2017) 04017014.
[16] N. Wiener, The average of an analytic functional, Proc. Natl. Acad. Sci. USA 7 (9) (1921) 253–260.
[17] M. Chaichian, A. Demichev, Path Integrals in Physics, Vol. I: Stochastic Processes and Quantum Mechanics, Institute of Physics Publishing, Bristol and Philadelphia, 2001.
[18] A.F. Psaros, O. Brudastova, G. Malara, I.A. Kougioumtzoglou, Wiener path integral based response determination of nonlinear systems subject to non-white, non-Gaussian, and non-stationary stochastic excitation, J. Sound Vib. 433 (2018) 314–333.
[19] I. Petromichelakis, R.M. Bosse, I.A. Kougioumtzoglou, A.T. Beck, Wiener path integral most probable path determination: A computational algebraic geometry solution treatment, Mech. Syst. Signal Process. 153 (2021) 107534.
[20] I. Petromichelakis, A.F. Psaros, I.A. Kougioumtzoglou, Stochastic response determination of nonlinear structural systems with singular diffusion matrices: A Wiener path integral variational formulation with constraints, Probab. Eng. Mech. 60 (2020) 103044.
[21] I. Petromichelakis, A.F. Psaros, I.A. Kougioumtzoglou, Stochastic response determination and optimization of a class of nonlinear electromechanical energy harvesters: A Wiener path integral approach, Probab. Eng. Mech. 53 (2018) 116–125.
[22] I. Petromichelakis, A.F. Psaros, I.A. Kougioumtzoglou, Stochastic response analysis and reliability-based design optimization of nonlinear electromechanical energy harvesters with fractional derivative elements, ASCE-ASME J. Risk Uncertain. Eng. Syst. B. Mech. Eng. 7 (1) (2021) 010901.
[23] I. Petromichelakis, I.A. Kougioumtzoglou, Addressing the curse of dimensionality in stochastic dynamics: A Wiener path integral variational formulation with free boundaries, Proc. R. Soc. Lond. Ser. A Math. Phys. Eng. Sci. 476 (2020) 20200385.
[24] A.F. Psaros, I.A. Kougioumtzoglou, I. Petromichelakis, Sparse representations and compressive sampling for enhancing the computational efficiency of the Wiener path integral technique, Mech. Syst. Signal Process. 111 (2018) 87–101.
[25] I.A. Kougioumtzoglou, I. Petromichelakis, A.F. Psaros, Sparse representations and compressive sampling approaches in engineering mechanics: A review of theoretical concepts and diverse applications, Probab. Eng. Mech. 61 (2020) 103082.
[26] A.F. Psaros, I.A. Kougioumtzoglou, Functional series expansions and quadratic approximations for enhancing the accuracy of the Wiener path integral technique, J. Eng. Mech. 146 (7) (2020) 04020065.
[27] A.F. Psaros, Y. Zhao, I.A. Kougioumtzoglou, An exact closed-form solution for linear multi-degree-of-freedom systems under Gaussian white noise via the Wiener path integral technique, Probab. Eng. Mech. (2020) 103040.
[28] M. Grigoriu, Stochastic Calculus: Applications in Science and Engineering, Springer, Berlin, 2002.
[29] F. Langouche, D. Roekaerts, E. Tirapegui, Functional integrals and the Fokker-Planck equation, Il Nuovo Cimento B (1971-1996) 53 (1979) 135–159.
[30] H. Risken, The Fokker-Planck Equation: Methods of Solution and Applications, Springer, Berlin, 1984.
[31] I.M. Gelfand, S.V. Fomin, Calculus of Variations, Prentice Hall, Englewood Cliffs, NJ, 1963.
[32] G. Strang, Introduction to Linear Algebra, Fifth ed., Wellesley-Cambridge Press, Wellesley, MA, 2016.
[33] M.I. Katsidoniotaki, A.F. Psaros, I.A. Kougioumtzoglou, Uncertainty quantification of nonlinear system stochastic response estimates based on the Wiener path integral technique: A Bayesian compressive sampling treatment, Probab. Eng. Mech. 67 (2022) 103193.